Scientific Spokesperson
R. Brock
Physics and Astronomy Department
Michigan State University
East Lansing, MI 48824
Phone 8-(517) 353-1693

Proposal to Study High Energy Neutrino Interactions with the Tevatron Quadrupole Triplet Beam

D. Bogert, R. Burnstein†, S. Fuess, J. Morfin,
L. Stutte*, J. K. Walker, H. Weerts
Fermi National Accelerator Laboratory
Batavia, IL 60510

W. Busza, J. I. Friedman, M. C. Goodman, H. W. Kendall, T. Lyons
L. Osborne*, R. Pitt, L. Rosenson, R. Verdier, S. Whitaker
Massachusetts Institute of Technology
Cambridge, MA 02139

M. Abolins, R. Brock*, D. Owen
Michigan State University
East Lansing, MI 48824

F. E. Taylor*
Northern Illinois University
DeKalb, IL 60115

February 1983

†Permanent Address: Illinois Institute of Technology, Chicago, IL
*Co-spokesperson

Contents

I. Introduction

Higher energy accelerators enable experiments to be done in kinematic regions where new thresholds may open and shorter distances may be probed. The results of such exploration are gratifying when the anticipated is confirmed - but exciting when the unexpected occurs. The higher energies available at the Tevatron could be particularly important for neutrino experiments since it may provide access to new physics most easily reached via the weak interaction. It is for these reasons that initial Tevatron running with a neutrino beam of high energy and high intensity is desirable. Such a beam - the Quadrupole-Triplet Beam (QTB) - has been designed[1] and is scheduled for running in the first ≈1 TeV running period.[2]

Searching for the unusual in neutrino physics requires a detector which is capable of yielding full kinematic information and which is sufficiently massive to yield events at the highest beam energies. The Flash Chamber- Proportional Tube Calorimeter in Lab C with $\approx 4 \times 10^5$ 5mm x 5mm x 3m cells and 340 metric tons of target is such a detector. Accordingly, we propose to do an experiment in the spirit suggested above: an experiment designed to check conventional results at new energies and to be sensitive to the possibility of detecting new physics.

In the search for possible anomalies at high energy, it is reasonable to check a variety of neutrino interactions. We intend to consider the following items in devising our triggers and in guiding our analysis:

1) Sensitive tests of the x-dependence of neutral currents are of

interest at high energies. The analysis of data taken less than a year ago with the Lab C detector is in progress with results expected soon. Running in a wide band beam will extend this analysis providing a first look at the x-dependence of neutral currents as compared to that of charged currents at very high energies. This can be done uniquely in this detector because of the capability to measure the transverse "energy" component of hadronic showers. These data will lead to a determination of $\sin^2\theta_w$ by measuring the neutral to charged current ratio.

2) Observation of the inverse muon decay reaction

$$\nu_\mu e \rightarrow \mu^- \nu_e$$

has been published for low energy neutrinos. The high energy of the QTB, the linear energy dependence of the cross section, and the energy independence of the quasi elastic background make this a clean check of the fundamental V-A structure of the weak interaction in this experiment.

3) Multimuon final states in neutrino physics have been studied for years and the conclusions are still in some instances unclear. Opposite sign dimuons have been throughly studied at CERN and are consistent with charmed quark production. However, like sign dimuon production appears to not be as well understood. Furthermore, a satisfactory explanation for the production of anomalously high energy trimuons seen in the HPWFOR experiment has not been made. Our ability to measure the muon final states as well as the missing transverse energy in such reactions may provide useful information in both of these instances.

Our previous experiment, E594, was an experiment of low counting rate in a dichromatic beam, but we have significant experience from engineering running in a wide band beam which had many events in each 1 msec spill. At that time we developed a variety triggers which exploited the pattern recognition capability of our proportional tube planes. We expect to extend that capability in this experiment over a range of energies of almost two orders of magnitude (≈5 to ≈500 GeV). This selective triggering capability is an essential feature of an experiment which addresses a wide variety of physics in a beam in which there are many events in each spill.

The hope in every search experiment at a new facility is that the unexpected may occur signaling the presence of new physics. While the anticipated running is not expected to be long (three months at last word[2]), our high event rates and excellent pattern recognition make the Lab C detector a natural choice for recognizing new phenomena. Also, our acquaintance with the device and the existence of extensive off-line analysis machinery will make it possible for us to respond quickly to anything unusual and exciting.

II. Physics With High Energy Neutrinos

In this section we describe the physics topics that will guide our triggering and analysis. In our calculations we have used the 300 GeV tune of the QTB shown in Figure 1. Also shown in that figure is the 600 GeV tune which has a higher fraction of very high energy neutrinos but substantially lower rates than for the 300 GeV tune out to $E_\nu \simeq 450$ GeV.

A. Neutral Current-Charged Current Comparisons

An important test of the quark structure of the nucleon can be made by comparing deep inelastic charged current (CC) scattering with neutral current (NC) scattering. We will make two measurements involving a NC to CC comparison.

1. Determination of $\sin^2\theta_W$

The first test is a determination of the mixing parameter, $x_W \equiv \sin^2\theta_W$, by measuring the ratio

$$R = \sigma^\nu(\mathrm{NC})/\sigma^\nu(\mathrm{CC}).$$

We have estimated the correction that must be applied to the number of νNC events induced by the $\bar{\nu}$ in the beam. But, as shown in Figure 1, the $\bar{\nu}$ flux falls more rapidly with energy than the ν flux. Furthermore, the ratio $\bar{R}$ is relatively insensitive to x_W. These two

facts allow the $\bar{\nu}$ background to be estimated. We have calculated the precision with which we would measure R and the resulting uncertainty in x_W with the results shown in Table I for a run of 50K triggers and an assumed uncertainty of 50% in the background subtraction. Comparison for E_ν>400 GeV can then be made with the measurement of x_W which will be done with data taken with the same detector from E594 for E_ν<250 GeV.

2. x Distribution Comparison for NC to CC Scattering

In addition to determining x_W, the Lab C detector is capable of measuring distributions of hadronic showers in NC reactions. This is important as it allows for a first look at the quark momentum distributions as probed by high energy weak neutral currents. We can make this comparison by measuring the quantity

$$E_\perp = E_h \theta_h$$

where the angle is defined in Figure 2. This comes from the following considerations:

The Bjorken scaling variable x is defined as

$$x = Q^2/2M\nu \ .$$

In the small angle approximation

$$Q^2 \simeq E_\nu E_\nu' \theta_\nu$$

$$\simeq E_\nu E_h \theta_h \frac{E_h \theta_h}{E_\nu - E_h}$$

$$\simeq \frac{E_\perp^2}{(1-y)}$$

where y is defined as usual as $y = E_h/E_\nu$. In this approximation,

$$x \simeq \frac{E_\perp^2}{(1-y)} \cdot \frac{1}{2ME_\nu y}$$

In the parton model the double differential cross section for neutrino scattering can be written

$$\frac{d^2\sigma}{dxdy} = E_\nu \Sigma_i k_i f_i(y) q_i(x)$$

where the sum is over valence and sea quark flavors, the k_i are constants for CC and functions of x_W for NC scattering , $q_i(x)$ are the momentum distributions for the ith quark flavor, and the $f_i(y)$ depend on the helicities of the ν-quark scattering.

By using the above, the differential distribution for NC or CC scattering can be written as an integral over the beam flux $\phi(E_\nu)$:

$$dN/dE^2 = \text{constants} \int d_y dE_\nu \phi(E_\nu)(1/2M_y(1-y)) \Sigma k_i f_i(y) q_i(x) .$$

Quark and antiquark combinations can be formed from the sum and difference of the inelastic ν-nucleon structure functions $F_2(x)$ and $xF_3(x)$. To calculate the sensitivity in $E_\perp^2$ to the x distribution, a Monte Carlo simulation of NC and CC scattering was done using $\sin^2\theta_W = 0.225$ and the NC cross section predicted by the Standard Model. The parameter tested is the exponent, n, in the assumed parent distributions

$$F_2(x) = (1-x)^n$$

$$xF_3(x) = \sqrt{x}\,(1-x)^n$$

The ratio

$$R_\perp = \frac{\dfrac{dN(NC)}{dE_\perp^2}}{\dfrac{dN(CC)}{dE_\perp^2}} \quad \begin{matrix} (n \text{ varied}) \\ (n=3) \end{matrix}$$

was calculated for n varied for NC (numerator) from n = 2 to 4. Even though the Jacobian mixes the x and y dependences, sensitivity to $(1-x)^n$ remains.

Figure 3 shows the parent x distribution for n = 2,3 and 4 and Figure 4 shows the results of the $E_\perp^2$ distribution using the measured experimental resolutions and 50K CC events. These curves were calculated for $E_h>20$ GeV. Increasing the cut to $E_h>100$ GeV does not affect the statistical errors beyond $E_\perp^2 \simeq 70$ GeV^2 where the effect is largest.

This neutral current to charged current comparison will require an understanding of the contamination of the $\bar{\nu}$NC in νNC. Indications are from the 300 GeV tune study that the small contamination at the higher neutrino energies translates into a small background at high $E_\perp^2$ because of the $\bar{\nu}$-y distribution. It is in precisely this high $E_\perp^2$ region where the experiment is most sensitive to n. By using the calculated deviation from flatness in the NC to CC ratio we conclude that Δn can be distinguished to at least ± 1.0. Changes in $\sin^2\theta_W$ effect only the overall value of the ratio, and not the $E_\perp^2$ dependence and the flux is not an influence on our sensitivity. This quantity will be measured along with the absolute structure

functions in our future dichromatic beam run (E649), but this will provide a sensitive first look at the NC x dependence at very high energies.

B. Elastic Neutrino Scattering

In addition to measuring deep inelastic neutrino reactions, the Flash Chamber-Proportional Tube Calorimeter is well suited to studying reactions which require sensitivity to very little energy deposition. We describe here two reactions which require rejection of backgrounds processes with only a few extra tracks.

1. Quasi-Elastic Scattering

In our 1981 wide band engineering running we successfully developed a trigger for the quasi-elastic (QE and $\overline{\text{QE}}$) reactions

$$\nu n \rightarrow \mu^- p \qquad \text{and}$$

$$\nu p \rightarrow \mu^+ n$$

In that experiment we used these events to monitor the neutrino flux shape which was possible because at the level of our background rejection, only exclusive channels with energy independent cross sections are thought to contaminate the true QE sample. The results of this measurement are shown in Figure 5 along with shape of the acceptance-corrected, energy unweighted CC events.

We have also triggered on this reaction in E594 where we know the incident neutrino energy. From these data we will measure the normalization factor necessary to determine the absolute flux. By using this normalization, we will be able to measure the flux of the QTB. Figure 6 shows our expected statistical precision in measuring the shape of the 300 GeV tune. From these data, we expect to be able to extend the determination of the energy dependence of

$$\sigma(\nu N \rightarrow \mu^- X)/E_\nu \text{ vs. } E_\nu$$

to a level of about 10% between E_ν of 250 and ≃400 GeV.

Our precision in flux determination at higher energies is not good, but, using the Atherton data[3] for secondary production and the parameterization and fits of Malensek[4] we expect to get a guide to the shape at very high energies by extrapolating our higher statistics QE-data from energies less than about 250 GeV. For example, the most sensitive parameter in the Atherton/Malensek fit is α in $(1-x_F)^\alpha$. Allowing α to vary ±10%[5] would extrapolate to an uncertainty in the QTB shape at 500 GeV of ≃±15-20%.

A typical example of a QE candidate is shown in Figure 7. Our level of discrimination is shown on Figure 8a which is not a quasi-elastic event as can be seen from the expanded view in Figure 8b showing more than just a proton at the vertex. Software pattern recognition discriminates at this level avoiding the contamination of elastic channels with low energy inelastic reactions.

2. Inverse Muon Decay

Our trigger for quasi elastics will also be sensitive to the inverse muon decay, (μ^{-1}) reaction:

$$\nu_\mu e \rightarrow \mu - \nu_e .$$

Observation of this reaction based on a comparison of QE and QE from CERN has been published.[6] The cross section for this reaction can be written in terms of the neutrino helicity and for general V and A as[7]

$$d\sigma/d(\cos\theta^*) \propto T(s)\{(1+p)(1-\lambda)A+4s^2(1-P)(1+\lambda)\}$$

where θ^* is the center-of-mass muon angle,

$$A = [s+m_e^2-(s-m_e^2)\cos\theta^*] \cdot [s+m\mu^2-(s-m_\mu^2)\cos\theta^*],$$

and $T(s) = (s-m_\mu^2)^2/32s^3$ which involves a substantial kinematic threshold suppression. The shape of $T(s)/\sqrt{s}$ is shown in Figure 9, and P = 1(-1) for LH (RH) neutrinos and λ=1(-1) for V-A (V+A). Because of the energy dependence of the cross section and the threshold effect, a high energy beam is well suited to producing this reaction.

The major background is from QE which is substantial at low energy. But, by measuring the square of the perpendicular component of the muon momentum, we expect to see the signal above a flat background. Figure 10 shows the combined $P_\perp^2$ distribution for an experiment with QE plus μ^{-1} events (V-A: open circles, V+A: crosses) as compared to the QE distribution alone. These data are normalized to the expected number of events (see Table IV) and include Fermi

motion, Pauli suppression, and resolution smearing for the muon angle and momentum (see Appendix A). By comparing with the shape from QE (for which there is no μ^{-1} analog) or with well understood theory we can then make a background subtraction.

By normalizing with our QE sample which we will do experimentally through the E594 data, we are independent of its Lorentz structure and hence sensitive only to the VA content of the μ^{-1} sample. Analyzed in this manner we will set a 90% confidence limit of $\lambda>0.6-0.7$ depending on the method of background subtraction and assuming P=-1. The best published results are from CHARM[6] which are $\lambda>0.4$ at lower energies.

As we explained earlier, we intend to use the QE data to measure the neutrino flux shape. Because μ^{-1} will be an unobservable background for this particular analysis, it is important to address the question of how this affects the flux determination. Two points help in this regard. First, the total number of events expected is smaller than the QE sample (see Section IIIB and Table III):

$$N(\mu^-)/N(QE) \simeq 0.17.$$

Secondly, the flux-dependence is determined by measuring the muon energy, $E_\mu(QE)$ and making the assumption

$$E_\nu = E_\mu(QE)$$

which involves only a small error because the q^2 transferred to the nucleon is small. The same identification would be made for the μ^{-1} events except then the actual E_ν is greater than $E_\mu(\mu^{-1})$ because of the missing neutrino. Therefore, the lower energy QE sample is

contaminated where the QE statistics are large. Figure 11 shows a calculation of the energies for QE alone (open circles) and QE plus μ^{-1} (closed circles). The dashed curve is the true shape of the 300 QTB spectrum drawn on top of the closed circle data to match in the 200-400 GeV region. Clearly, our ability to determine the shape is not compromised significantly by the μ^{-1} sample measured as if they were from QE events.

C. Multi-Muon Phenomena

One of the expected signals for the opening of a new quark channel is the presence of additional muons relative to that associated with the primary vertex. Production of $\mu^+\mu^-$ pairs, for example, in ν_μ experiments was recognized early to be evidence for the opening of the charmed quark channel in the reaction

$$\nu_\mu (d \text{ or } s) \rightarrow \mu^- c\, X$$
$$\qquad\qquad\qquad\quad \big\lfloor \rightarrow \mu^+ s \nu_\mu$$

This reaction and its charge conjugate partner in ν_μ beams have been studied extensively by all electronic experiments with thousands of events collected in the world's data.[8]

In addition to opposite-sign dimuon events, events with $2\mu^-$ have also been observed by all electronic experiments.[9] Figure 12 shows

the $\mu^-\mu^-/\mu^-$ rate for the world's data [10] demonstrating that substantial disagreement persists: the CDHS rates are almost an order of magnitude lower than that for HWFOR and CFNRR, which are in basic agreement with one another. Not only are experiments in disagreement but there appears to be confusion yet as to the mechanism thought to be responsible for $\nu_\mu \rightarrow \mu^-\mu^-$.[10] One of the possible sources was thought to be associated charmed particle production:

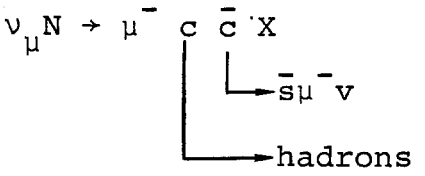

However, first order QCD bremmsstrahlung into cc pairs is calculated to be less than 10^{-5} at all neutrino energies.

In addition to $\mu^-\mu^+$ and $\mu^-\mu^-$ final states all experiments have reported observation of $\mu^-\mu^-\mu^+$ final states (and some 4μ final states).[11] While calculations have suggested that the source of such events is likely a conventional QED radiative mechanism[12], there are published reports of events in the 400 GeV proton energy QTB at Fermilab with substantial momentum in the muons (>230 GeV/c) and missing transverse momentum.[13]

Should the rate for these so-called "super" trimuons persist, unchanged, to the QTB energies, we might expect to produce ≈3 such events in a three month run. On the other extreme, should the production of top quarks occur, there might be the additional production of trimuons (and 4 muons!) from the reactions and decays

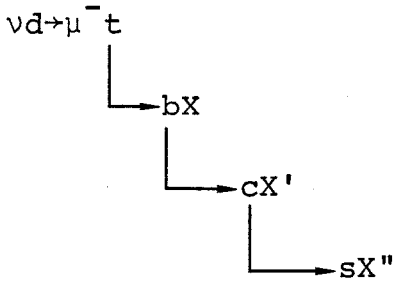

where X,X', and X" could each have muons from semileptonic decays. Using the Kobayashi-Maskawa[14] mixing angles $\theta_1 \approx 13^\circ$, $\theta_2 < 30^\circ$, and $\theta_3 < 16^\circ$, 10% semileptonic branching ratios, and an approximate $m_T \approx 20$ GeV/c^2 we estimate less than 10 events with 3 muons.

Gottschalk[15] has suggested that it is difficult to account for the "super" events with the successful arguments applied to the other 3μ data. These events could be the first indications of the opening of a new threshold and hence we might expect more than the few events mentioned above. Should this be the case, we could add important new information to th issue because of our good containment and hadronic shower-angle sensitivity. Due to the lower energy of the CERN neutrino beam, these events would not have been

observed in the CDHS experiment.

We have calculated the trigger rate for muons from π and K decays which is shown in Figure 13 along with measured rates from other experiments[10]. Our calculation was done with a Monte Carlo simulation of shower cascades in the Flash Chamber-Proportional Tube Calorimeter. Also, shown is the result of a simple model which can be parameterized as

$$\text{probability of } \mu^- \text{ production} = 0.00122\ E_h/E_\mu{}^2 \text{ (in GeV)}$$

which gives us an estimate for the probability for background dimuons integrated over the neutrino spectrum as

$$1.05/E_\mu{}^2 \text{ \% per CC event.}$$

By demanding TM_i (see Appendix A, Section h) be satisfied up to and including the third toroid plane we would be imposing a minimum 10 GeV/c muon momentum cut on the second muon. Then the background + charm rate will be approximately 0.3 events/spill.

There are still open questions in multimuon physics which are appropriate to further study in a higher energy beam in which a few hundred same-sign dimuons plus more than 50 trimuons would be expected (see Section III B.). A 3 month QTB run may be sufficient to shed some more light on these issues.

D. Unusual Reactions

We conclude this section by discussing briefly the diverse event topologies that may be detected in a fine grain calorimeter.

The CDHS experiment has seen 45 ± 13 examples of ψ/J production by making mass combinations of their $\mu^+\mu^-$ data.[16] By using their measured cross section, we might expect approximately 50 events of the type (with an 8% BR to $\mu\mu$)

$$\nu N \rightarrow \nu \psi X \quad (\psi \rightarrow \mu^+\mu^-)$$

In addition to measuring the μ pair kinematics in such events, might be useful information in the hadronic debris.

The CHARM collaboration has reported some evidence (1.7 ± 1.7 events) for coherent μ pair production ("tridents") from the nuclear field:[17]

$$\nu_\mu Z \rightarrow \nu_\mu \mu^+ \mu^- Z.$$

Because this reaction is coherent, essentially no hadronic energy should appear in the calorimeter. As discussed earlier with regard to QE discrimination, we should be able to reject backgrounds to the trident reaction by eliminating events with slow hadrons at the vertex. Approximately 20-30 such events should be made in our steel shot target planes in this run. The purely charged current process

$$\nu_\mu Z \rightarrow \mu^- e Z$$

should occur at a slightly higher rate. Also, μe final states in high excess of expectations have been reported for years from low energy counter experiments at CERN and BNL.[18] Our ability to detect these final states is good.

By using the flux information discussed above and conmbining the neutrino and antineutrino CC events, the integral of F_2 could be isolated. An interesting flux integrated CC measurement would be then to test for additional constituents in the nucleon. For example,[19]

$$r = \lim_{Q^2 \to \infty} \int dx\ F_2(x,Q^2) = \frac{3f}{16+3f}$$

where f is the number of quark flavors: for f = 6, r = 0.529, for f = 8, r = 0.600. As a function of Q^2 this would appear as a rise to a new value. A competing effect might be the presence of speculated objects such as the gluino. For this situation,

$$r' = \frac{3f}{16+3f+18}$$

and a drop in $\int dx\ F_2(x)$ would occur at the scale of the gluino mass squared.

We can reconstruct dimuon states and can detect them whether produced in the calorimeter or upstream. Timing information coupled with the good muon angular resolution may allow us to make mass combinations of muon pairs originating from neutrino interactions (or whatever) upstream and possibly point them back to their point of origin.

III. Plan of the Experiment

In this proposed experiment in which rare and frequent triggers are allowed to compete, a versatile triggering system must be employed. In our engineering run we devised a dynamic trigger gating system which we will use in the QTB. Figure 14 shows schematically how this was arranged. In a) we show the decay muon spectrum in time obtained from scintillation counters placed in the berm. By scaling the average counts from these signals we allowed rare triggers to compete in the first 80% of the spill (Figure 14b). At the end of this 80% gate, if no rare trigger requirements were satisfied, we enabled a second gate, (Figure 14c) the 20% gate, in which a minimal trigger was added to the allowed combinations. This 80%/20% division was devised in order to obtain rare and desired events with high efficiency yet have a sample order of all events produced.

In order to minimize trigger dead time, rare triggers will be allowed to compete with one another during a Rare Gate - and with an Open Trigger during the latter part (Open Gate) of the spill. The gate width will be designed to take at least one deep inelastic charged or neutral current trigger.

A. Proportional Plane Triggering

The fine segmentation of the target proportional tube planes and the electronics provide the means of generating different signals

which can be combined into physics triggers. (The trigger signals are described in Appendix A, Section h.) These signals can be combined to provide triggers on shower energy (maximum or minimum), shower width, shower length, the absence of any muon, or the presence of one, or more than one muon. It should be emphasized that this is a technique we have successfully used in the past and will easily translate to an experiment in the QTB.

The types of triggers envisioned are:

Rare Gate Triggers

- Very high energy CC. This trigger requires a muon satisfying MS and a $\Sigma\Sigma$(total energy deposition) above some predetermined amount.
- Quasi-elastic. This trigger requires that no more than the minimum ionization of a muon traversing the calorimeter be deposited and that there be a muon traversing the toroids (about 15 GeV/c minimum). The measured trigger efficiency as a function of vertex position is shown in Figure 15 for the 1981 engineering run.
- Very high energy NC or CC. This trigger requires only a minimum $\Sigma\Sigma$.
- Multimuon. This trigger will involve a coincidence of TM_j for all toroid planes and AM_i for the calorimeter signifying the presence of two or more muons from an event.
- Prescaled Open Triggers. These triggers might be of various types to check for systematic biases due to other trigger requirements. The prescaling would be set to minimize dead time and yet provide enough of a sample to be useful later in cross-checking.

Open Gate Triggers

Open Triggers are formed by all events occuring in the calorimeter with only a minimal $\Sigma\Sigma$ as requirement.

We will rely on the flash chambers to search for and detect any unusual event topologies as well as for shower angle measurement, energy measurement, event type identification, etc.. It is useful, however, to have at least a characterization of all events (1/2 M in total). We have devised a scheme to allow individual Σ_i from each plane and all toroid traversals to be read our for each event without triggering the flash chambers. These signals will be accumulated very fast (approximately 20 per fast spill) and therefore not have the resolutions obtainable from either the off-line flash chamber or proportional plane data. We will use these data to aid in correcting for acceptance and efficiency losses. The data acquisition scheme envisages the storage of this information into fast memories which can be read into the computer at the end of each spill. This acquisition is expected to take about 5 μsec resulting in negligible dead time.

Table II shows the expected trigger rates in the entire trigger volume (approximately a cylinder 1.8 m in radius and 17 m long) using 1×10^{13} protons per spill and the 300 GeV tune of the QTB.

B. Event Rates

The expected number of useable events which would occur in 1 x 10^{13} protons on target inside the Lab C detector (radius = 1.3 m, length = 1680 cm) are listed in Table III for the 300 GeV tune of the QTB (Figure 1). For a short exposure of 5 x 10^{17} protons, or 50K spills (corresponding to roughly a 40% efficient three month run) with this beam we would collect the number of events shown in the left hand column of Table IV. The numbers in parentheses are the number of events expected for those reactions which produce more than one event per spill such that the total number of spills still totals 50K.

The amount of information which must be processed in the Lab C detector at trigger time is large. This means that we are limited to one event per fast spill. A scheme (subsequently named "ponging") was used during the last running period in N0 whereby 2 x 10^{12} protons were delivered in 5 separate short spills during the entire slow spill. Because of the 5 seconds presently required between flash chamber triggers, three such "pongs" could be arranged in the 10 second slow spill which has the effect of tripling the data for those reactions which were dead time limited. The rates which result are shown in the right hand column of Table III.

We show in Figure 16 the integral distributions for a) the fraction of neutrinos in the QTB and b) the number of QE events in 5 x 10^{17} protons on target. Figure 17 shows the integral distributions for a) the fraction of νCC events and b) the number of νCC events per 10^{13} protons. Note that from Figure 12 and Figure 17 we might expect $\approx$200 like-sign dimuon events E_ν>150 GeV.

IV. Requests

Here we list our requests for this proposed QTB experiment:

1. We request that approval be given to run the Lab C detector during the QTB planned for the first Tevatron running period.

2. We request that this running be for a minimum of three months and that the entire running period be at the 300 GeV tune setting of the QTB.

3. Because of inherent triggering and data-logging limitations, we request that extraction be done in three 1 msec spills separated by five seconds similar to the "ponged" extraction of 1982.

4. We request that 4 months before the end of the first Saver running period we be approved to bring up the Lab C detector.

5. In order to calibrate the calorimeter, calibrate the new drift system, and measure the muon production from high energy showers we request running time during the last 2 months of the first Saver run at which proton energies are expected to be increased beyond 400 GeV. We request that

the calibration beam line be capable of providing hadrons and muons at energies up to 400 GeV.

6. In order to utilize the pattern recognition capabilities of the Lab C detector, we request continued scanning time on the FAF PDP-11 computer system. Roughly seven months, full time scanning would be sufficient for 150,000 flash chamber triggers.

V. Conclusion

We believe that the running of the QTB as the first neutrino beam at the Tevatron is the best way to quickly explore new kinematic regions. The Lab C Flash Chamber-Proportional Tube Calorimeter can make important checks of neutrino physics in this new regime and is a detector capable of indicating the presence of new phenomena. A run of 3 months or longer would provide a usable number of rare events and very high energy deep-inelastic events.

References

1. L. Stutte, 1982 ν Beam Workshop, Fermilab, unpublished 1982.

2. T. Yamanouchi, ibid..

3. H. W. Atherton et al., "Precise Measurements of Particle Production by 400 GeV/c Protons in Beryllium Targets", CERN 80-07, 1980.

4. A. Malensek, "Empirical Formula for Thick Target Particle Production", FN-341, Fermilab, 1981.

5. A. Malensek, private communication.

6. J. V. Allaby et al., PL 93B, 203, 1980.
   N. Armenise et al., PL 84B, 137, 1979.

7. C. Jarlshog, Lett. Nuovo. Cim. IV, 377, 1970.

8. H. Abramowicz et al., Zeit. für Physik C 15, 19, 1982.
   A. Benvenuti et al., Phys. Rev. Lett. 34, 419, 1975.
   A. Benvenuti et al., Phys. Rev. Lett. 35, 1199, 1975.
   A. Benvenuti et al., Phys. Rev. Lett. 41, 1204, 1978.
   B. C. Barish et al., Phys. Rev. Lett. 36, 939, 1976.
   B. C. Barish et al., Phys. Rev. Lett. 39, 981, 1977.
   M. Holder et al., Phys. Rev. Lett. 69B, 377, 1977.

9. J. Knobloch et al., Proc. Neutrino '81 ed. R. J. Cence, E. Ma, A. Roberts, 1, 421. Maui, Hawaii, 1981
   M. Jonker et al., Phys. Lett. 107B, 241, 1981a.
   M. Holder, et al., Phys. Rev. Lett. 39, 433, 1977.
   T. Trinko et al., Phys. Rev. D23, 1889, 1981.
   M. H. Shaevitz et al., Proc. Summer Inst. Part. Phys. ed. A. Mosher, p. 475. Stanford, CA, 1980

10. H. E. Fisk, "Production of Charm and New Parciles in Neutrino Nuclear Interactions".
    H. E. Fisk and F. Sciulli, Ann. Rev. Nucl. and Part. Sci. 32, 499, 1982.

11. B. C. Barish et al., Phys. Rev. Lett. 38, 577, 1977.
    A. Benvenuti et al., Phys. Rev. Lett. 38, 1110, 1977.
    M. Holder et al., Phys. Lett. 70B, 393, 1977.
    T. Hansl et al., Nucl. Phys. B142, 381, 1978.
    A. Benvenuti et al., Phys. Rev. Lett. 42, 1024 (1979).

References (continued)

12. V. Barger et al., Phys. Rev. D18, 2308, 1978.

13. A. Benvenuti et al., Phys. Rev. Lett. 40, 488, 1978.

14. M. Kobayaski, K. Maskawa, Prog. Theor. Phys. 49, 652, 1973.

15. T. Gottschalk, Ph.D. Thesis, University of Wisconsin, unpublished, 1978.

16. J. Knoblock, Proc. of the 1981 International Conference on Neutrino Physics and Astrophysics, Maui, Hawaii, 1981.

17. N. Armenise et al., Proc. of Neutrino '79 Conference, Bergen, 1979.

18. H. Faissner et al., Proc. of Neutrino '78 Conference, Purdue University, 1978.
A. Bross, Ph.D. Thesis, University of Illinois, unpublished, 1977.

19. G. Barbiellini, DESY 79/67, 1979.

Table Captions

I. The precision expected in measuring $x_W = \sin^2\theta_W$ in an exposure of 5×10^{17} protons assuming a 50% uncertainty in the $\bar{\nu}$NC subtraction in the total NC sample for different neutrino energy regions.

II. Trigger rates per 10^{13} protons expected in a radius of 1.8m.

III. Events per 10^{13} protons in the 1.3m fiducial volume. The multimuon rates do not include meson decays.

IV. Expected number of events occuring in the Lab C detector fiducial volume of 1.3m radius in a 5×10^{17} proton exposure. The numbers in parentheses represent the number of each reaction collected for 50K spills total (1 spill per machine cycle) in the left hand column and 150K spills total (3 spills per machine cycle) in the right hand column.

	E_ν>200 GeV	>300	>400	>500	>600
νCC	8500	3700	1250	625	100
$\bar{\nu}$CC	1500	415	83	18	-
νNC	2600	1150	380	190	30
$\bar{\nu}$NC	670	154	30	~7	-
νNC/total NC	20%	12%	8%	~4%	-
$\frac{\delta x_W}{x_W}$	±13%	±8%	±7%	±9%	±21%

TABLE I

Trigger Rate Per 10^{13} Protons

$\nu CC+\bar{\nu}CC$	Total	17
	E_ν>100 GeV	10
	>200	6
	>300	4
	>400	1
	>500	0.4
$\nu CC+\bar{\nu}CC+\nu NC+\bar{\nu}NC$	Total	23
	E_H>100 GeV	6
	>200	2
	>300	0.5
	>400	0.1
$\nu n \rightarrow \mu^- p+\nu p \rightarrow \mu^+ n$		0.15
$\nu N \rightarrow \mu^- + >2\mu^- X$		<0.3

TABLE II

	Events Per 10^{13} Protons
νCC	10.8
$\bar{\nu} CC$	3.6
νNC	1.8
$\bar{\nu} CC$	0.6
$\nu n \rightarrow \mu^- p$	0.07
$\bar{\nu} p \rightarrow \mu^+ n$	0.03
$\nu_\mu e \rightarrow \mu^- \nu_e$	0.01
$^*\nu_\mu N \rightarrow \mu^- \mu^- X$	~0.01
$^*\nu_\mu N \rightarrow \mu^- \mu^- \mu^+ X$	~0.001

*does not include π/K decay

TABLE III

	Events in 1 msec Spill Per Cycle	Events in 3 1 msec Spills Per Cycle
νCC	540K (25K)	540K (75K)
$\bar{\nu}CC$	90K (8.3K)	90K (25K)
νNC	180K (8.3K)	180K (25K)
$\bar{\nu}NC$	30K (2.8K)	30K (8.4K)
$\nu n \rightarrow \mu^- p$	3.0K	3.0K
$\bar{\nu} p \rightarrow \mu^+ n$	1.0K	1.0K
$\nu_\mu e \rightarrow \mu^- \nu_e$	~600	~600
$\nu_\mu N \rightarrow \mu^- \mu^- X$	~500	~500
$\nu_\mu N \rightarrow \mu^- \mu^- \mu^+ X$	~50	~50

TABLE IV

Figure Captions

1. Neutrino and antineutrino fluxes for the 300 GeV (crosses) and 600 GeV (solid line) tunes of the QTB.
2. Definition of the angle θ_h between the center of gravity of the hadron shower and the incident neutrino direction.
3. Parent distributions for the NC Monte Carlo study: $F_2(x) = (1-x)^n$, n = 2 (dash-dot), 3 (dashes), and 4 (solid line). The curves are normalized to equal areas.
4. The calculated distribution in the ratio R_l (defined in the test) for various values of n. The statistical precision is indicated for an assumed 50K CC sample. $Sin^2\theta_W = 0.225$ was used in this calculation.
5. Measured neutrino flux shape using the QE sample (.), CC (∘), unweighted sample, and calculated shape. Data are from the 1981 engineering run.
6. Expected muon energy distribution from a 5×10^{17} proton exposure using the 300 GeV tune of the QTB. This shows the statistical precision for the flux shape expected in such a run.
7. On-line display of a true QE candidate from the Lab C detector.
8. On-line display of a potential QE candidate (a) and an expanded view of the vertex regions of this event (b) showing it to not be an example of $\nu_\mu n \rightarrow \mu^- p$.

Figure Captions (continued)

9. Normalized threshold factor, $T(s)/\sqrt{s}$, for the μ^{-1} reaction as a function of energy showing substantial suppression out to energies beyond typical horn beam fluxes.
10. Calculated perpendicular component of the negative muon from μ^{-1} + QE (V-A, o), μ^{-} + QE (V+A,x), and QE alone (solid curve). The statistics are those expected from a 5 x 10^{17} proton exposure.
11. Calculated muon energy distribution for QE (o) and μ^{-1} + QE (.). The dashed curve is the shape of the 300 GeV tune of the QTB drawn over the (.) points in the 200-400 GeV region. The statistics are those expected for a 5 x 10^{17} proton exposure.
12. Like-sign dimuon rates for neutrino experiments from Fermilab and CERN. Data taken from Reference 10.

13. Calculation of expected μ^{-} production rate as a function of hadron shower energy. The curves correspond to minimum muon energies 5, 10, and 20 GeV in a simple shower model. The data points are from a simulation of hadron cascades in the Lab C calorimeter. The crosses are μ^{-} greater than 10 GeV from primary pions using the fragmentation function $D_{\bar{q}}^{\pi^-}$ of Sehgal ("Hadron Production by Leptons", 1977 International Symposium on Lepton and Photon Interactions at High Energies, Hamburg, 1977). The dotted curves and dashed curves are from the CFRR and CDHS experiments respectively scaled to the Lab C detector average absorption length and $E_{\mu}>10$ GeV.

Figure Captions (continued)

14. An illustration of the trigger gating scheme used in the engineering run of 1981.
    a) Profile of decay muons from scintillators in the berm.
    b) Rare Gate covering approximately 80% of the spill.
    c) Open Gate covering the rest of the spill.
15. Measured trigger efficiency for QE and $Q\bar{E}$ triggers as a function of vertex positions from the 1981 engineering run.
16. Integral distributions for
    a) neutrinos from QTB
    b) QE events in a 5×10^{17} proton exposure
17. Distributions for
    a) Integral of CC events from a 5×10^{17} protons exposure
    b) Number of CC events per 10^{13} protons

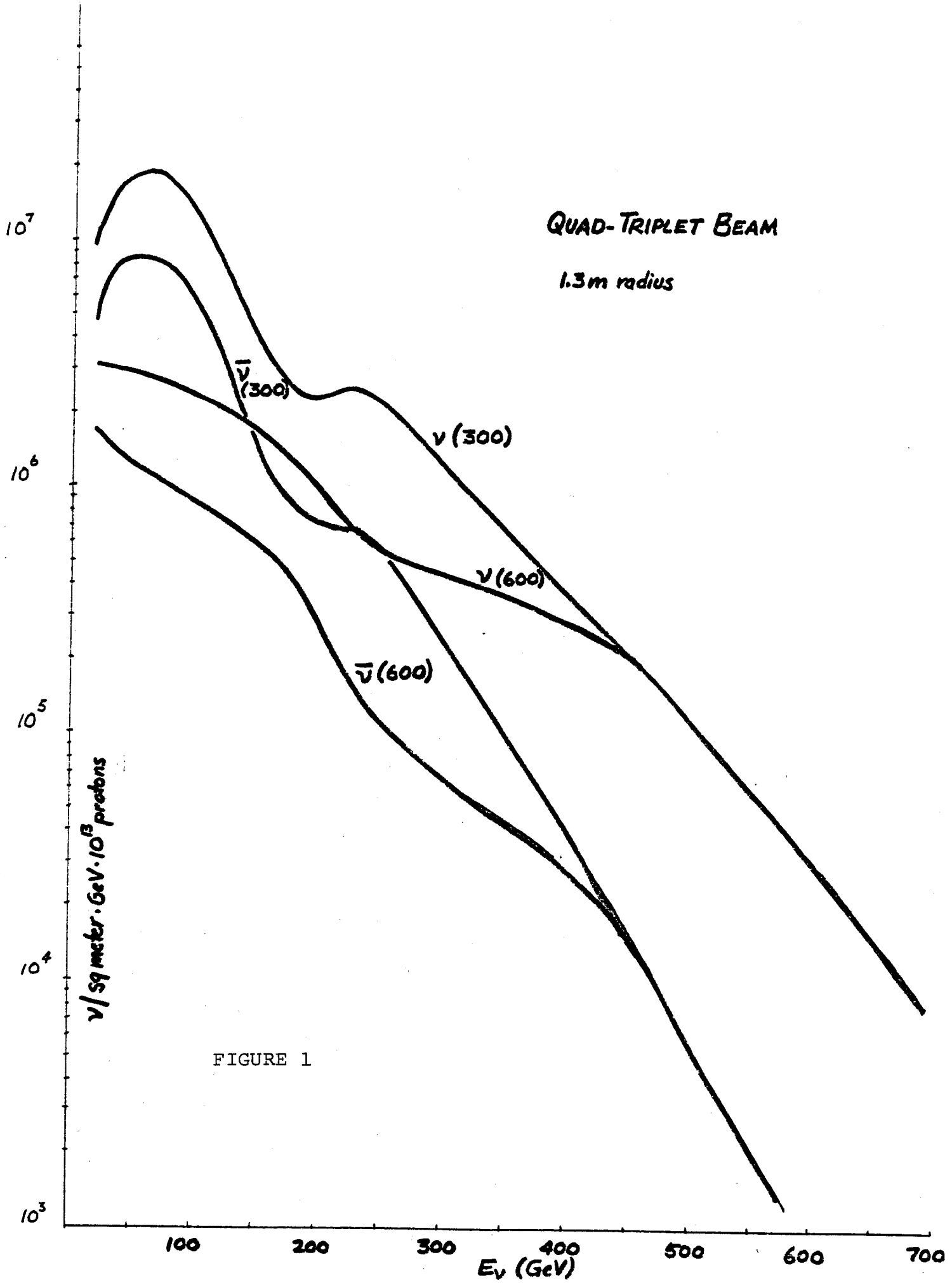
QUAD-TRIPLET BEAM
1.3m radius
$\bar{\nu}$ (300)
ν (300)
ν (600)
$\bar{\nu}$ (600)
10^7
10^6
10^5
10^4
10^3
ν/sq meter · GeV · 10^{13} protons
100
200
300
400
500
600
700
E_ν (GeV)

FIGURE 1

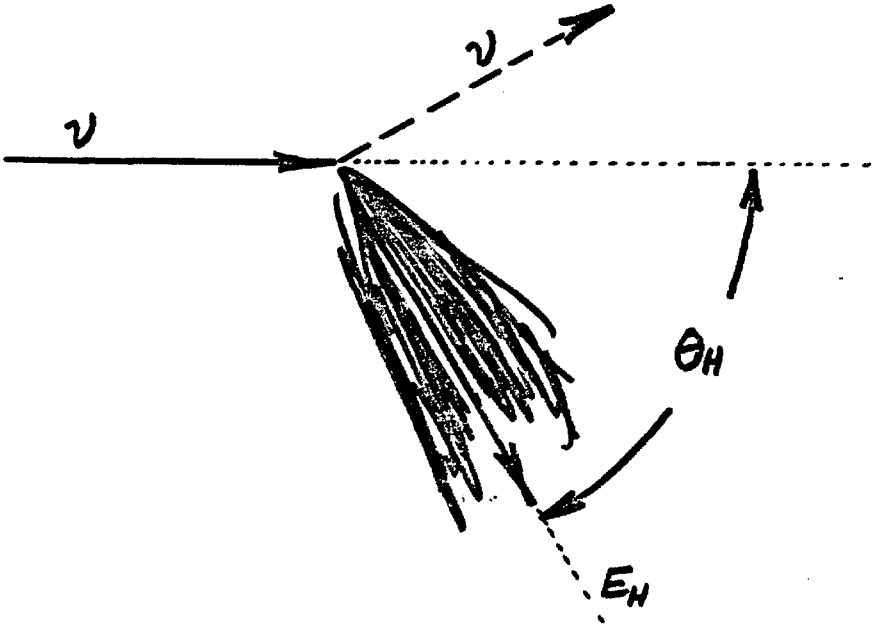

FIGURE 2

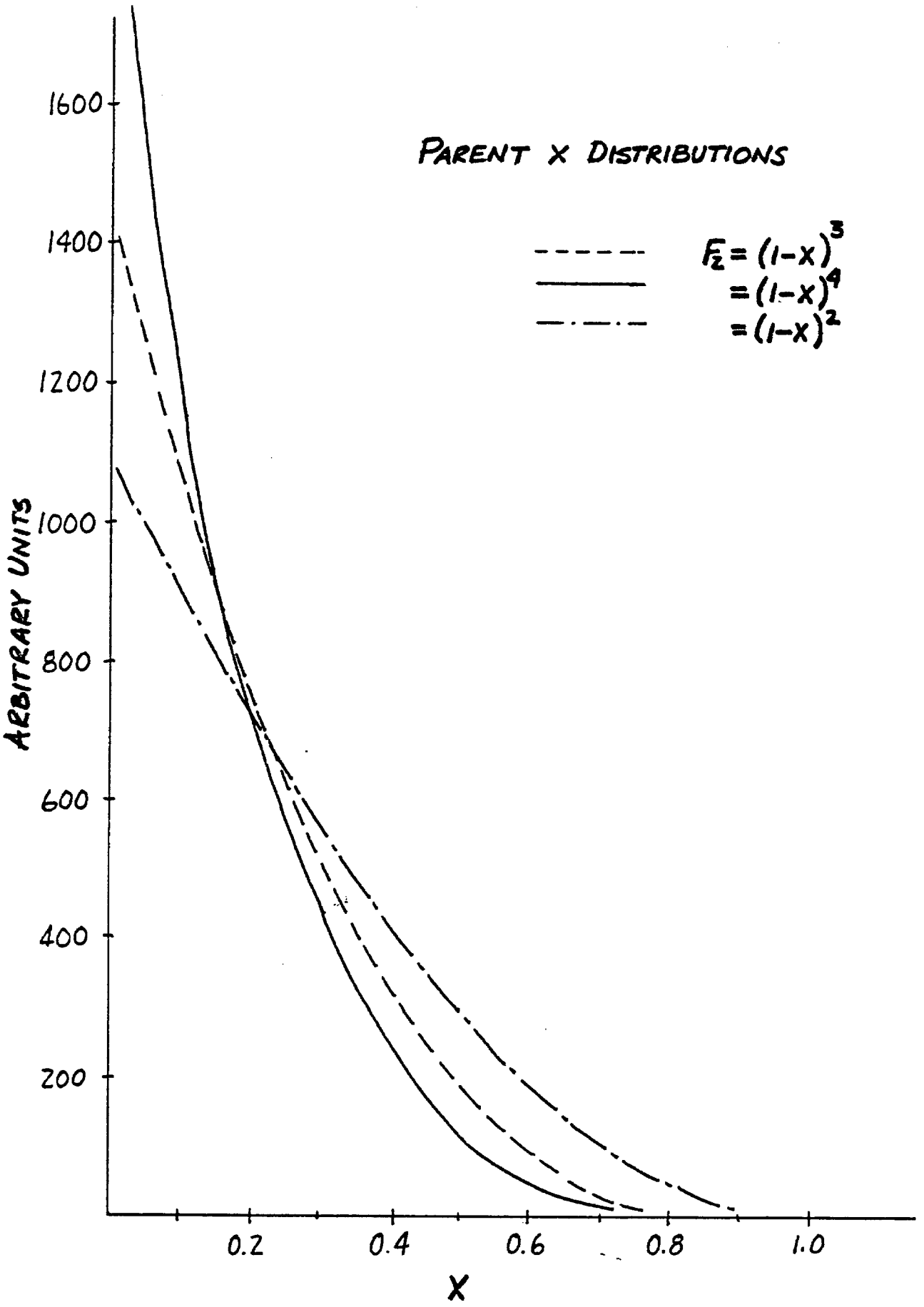
PARENT X DISTRIBUTIONS
$F_2 = (1-X)^3$
$= (1-X)^4$
$= (1-X)^2$
ARBITRARY UNITS
1600
1400
1200
1000
800
600
400
200
0.2
0.4
0.6
0.8
1.0
X

FIGURE 3

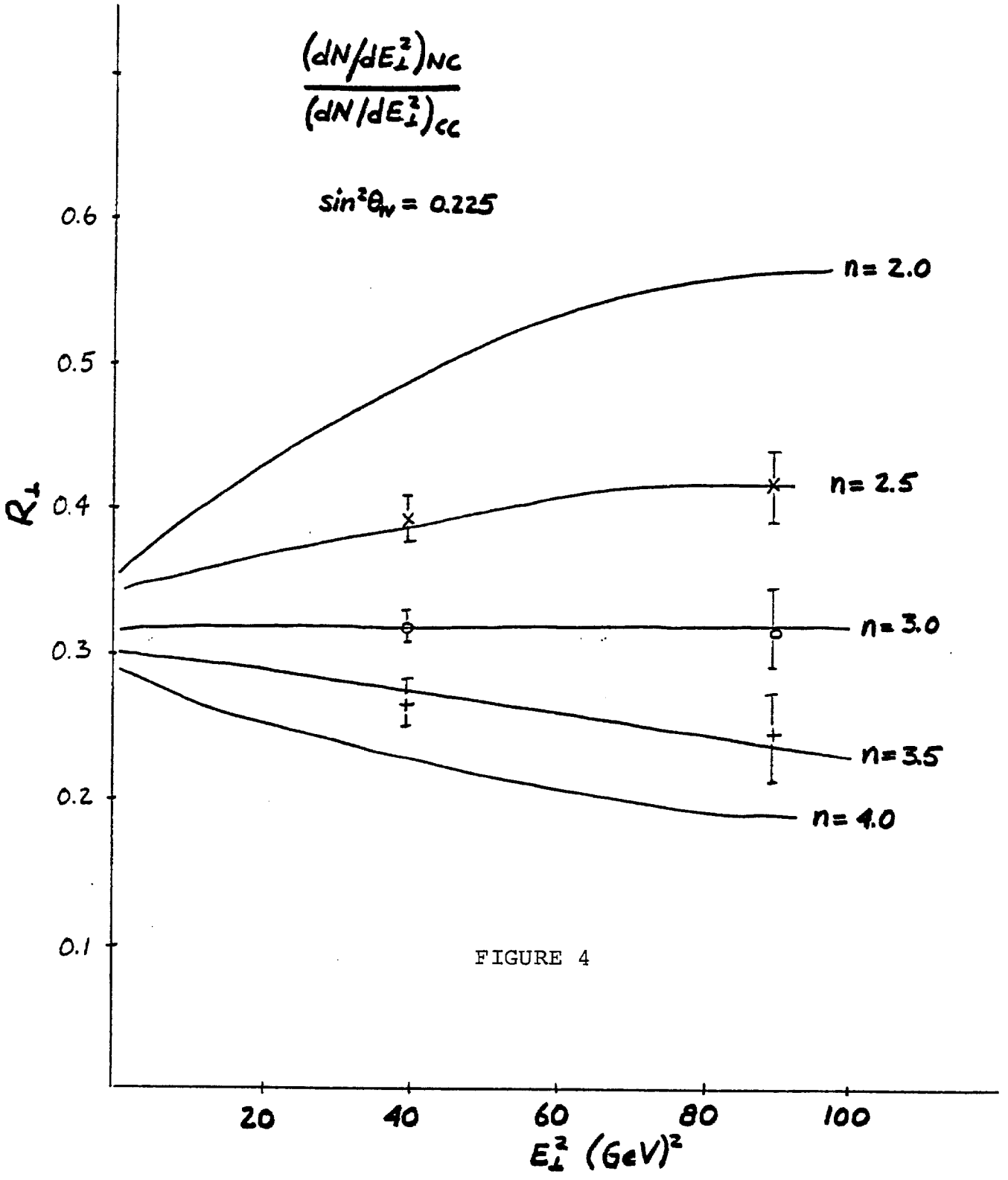
$\frac{(dN/dE_\perp^2)_{NC}}{(dN/dE_\perp^2)_{CC}}$
$\sin^2\theta_W = 0.225$
$R_\perp$
0.6
0.5
0.4
0.3
0.2
0.1
n= 2.0
n= 2.5
n= 3.0
n= 3.5
n= 4.0
20
40
60
80
100
$E_\perp^2$ (GeV)^2

FIGURE 4

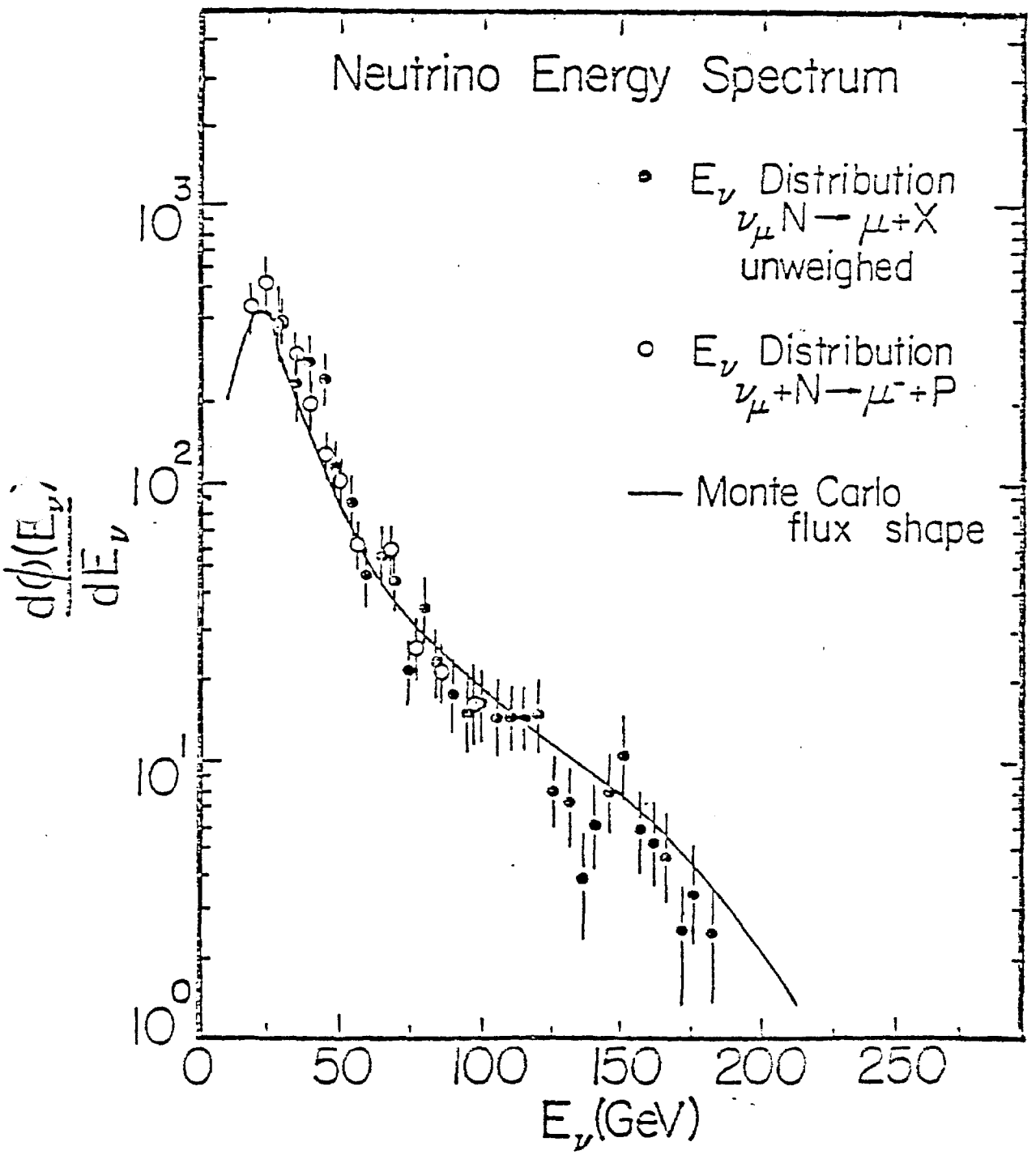
Neutrino Energy Spectrum
E_ν Distribution
$\nu_\mu N \rightarrow \mu + X$
unweighed
E_ν Distribution
$\nu_\mu + N \rightarrow \mu^- + P$
Monte Carlo
flux shape
$\frac{d\phi(E_\nu)}{dE_\nu}$
10^3
10^2
10^1
10^0
0
50
100
150
200
250
E_ν(GeV)

FIGURE 5

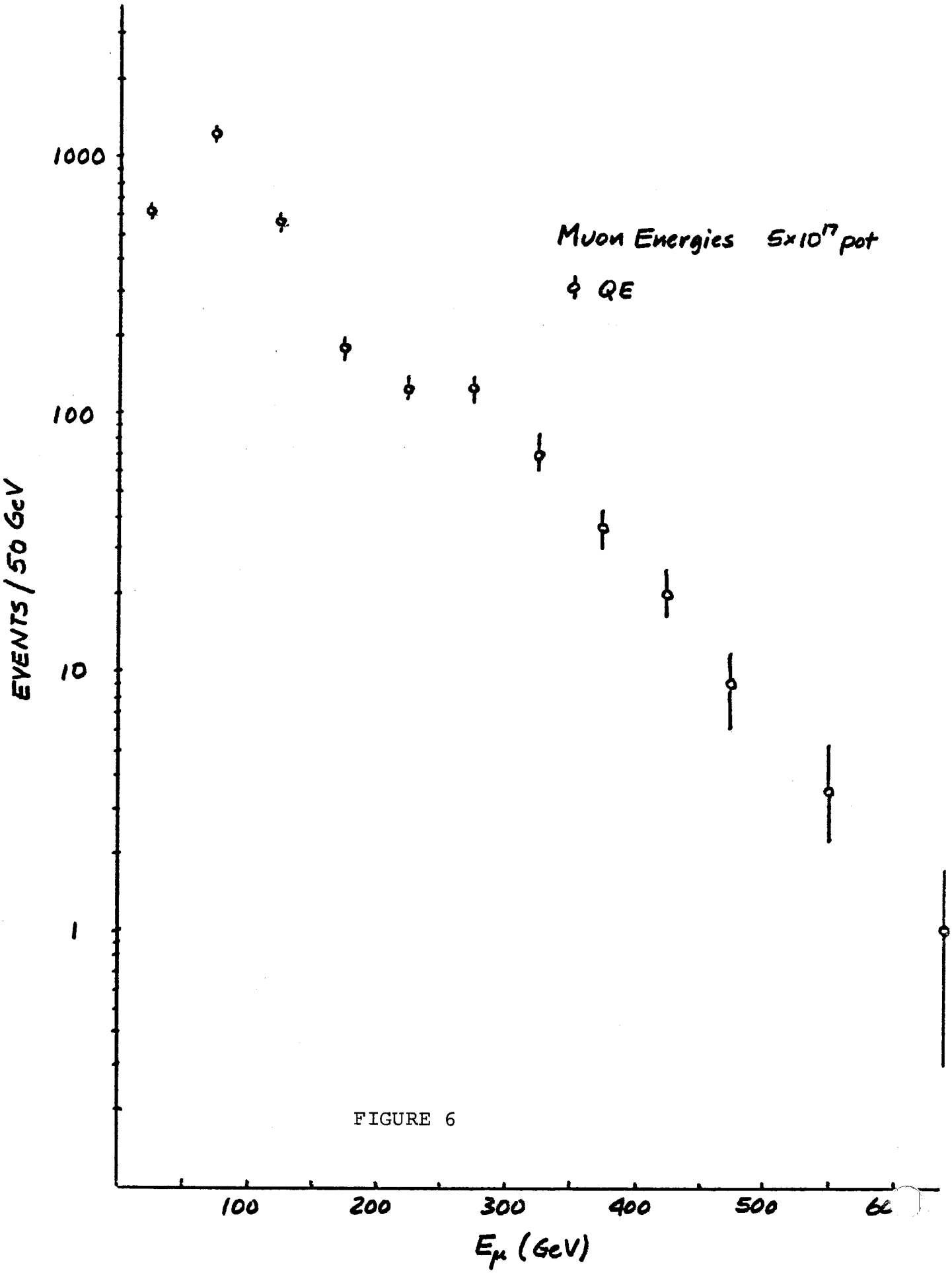
Muon Energies 5x10^17 pot
QE
EVENTS / 50 GeV
1000
100
10
1
100
200
300
400
500
E_μ (GeV)

FIGURE 6

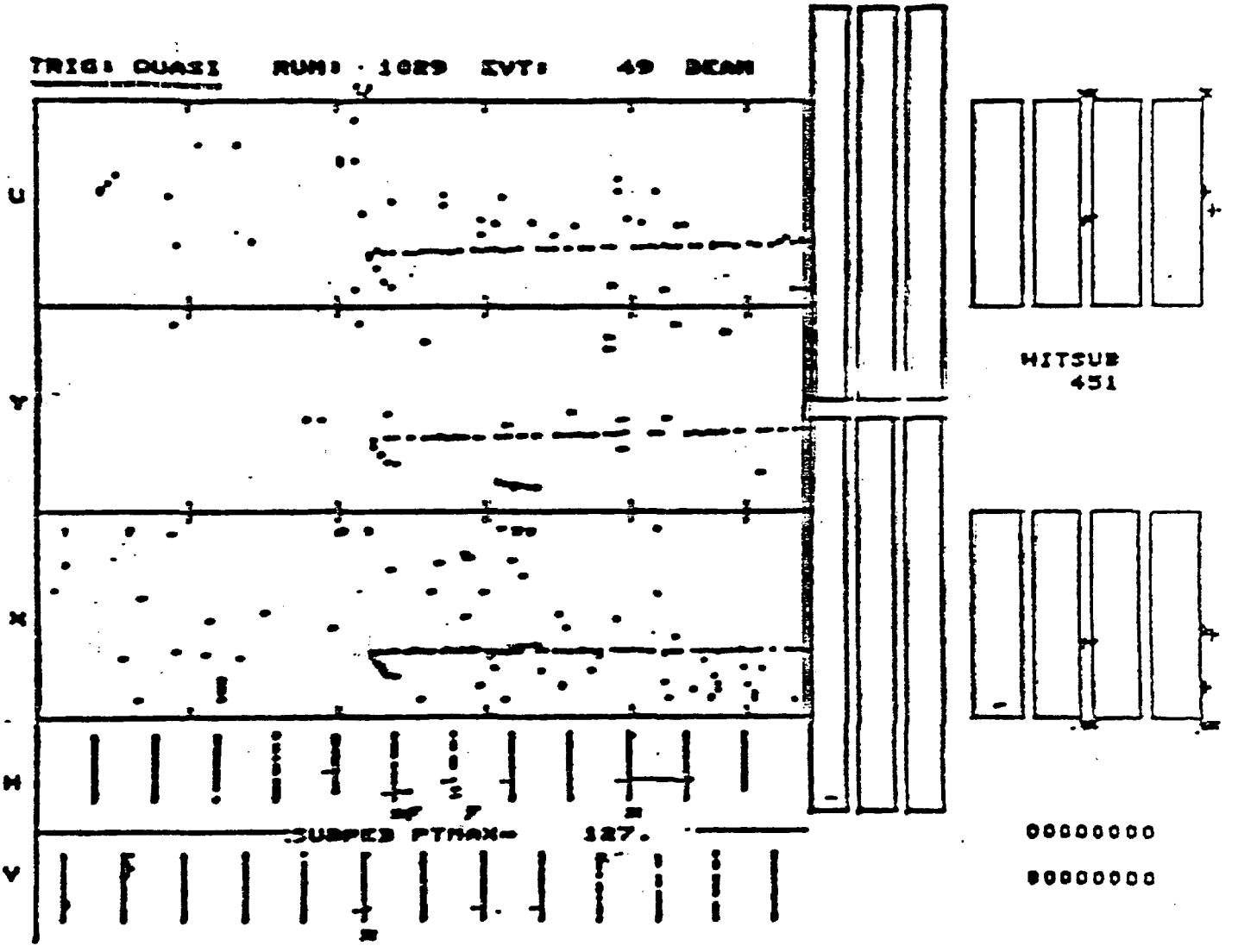
TRIG: QUASI
RUN: 1029 EVT: 49 BEAM
U
V
X
H
V
SUMPED PTMAX= 127.
HITSUB
451
00000000
00000000

FIGURE 7

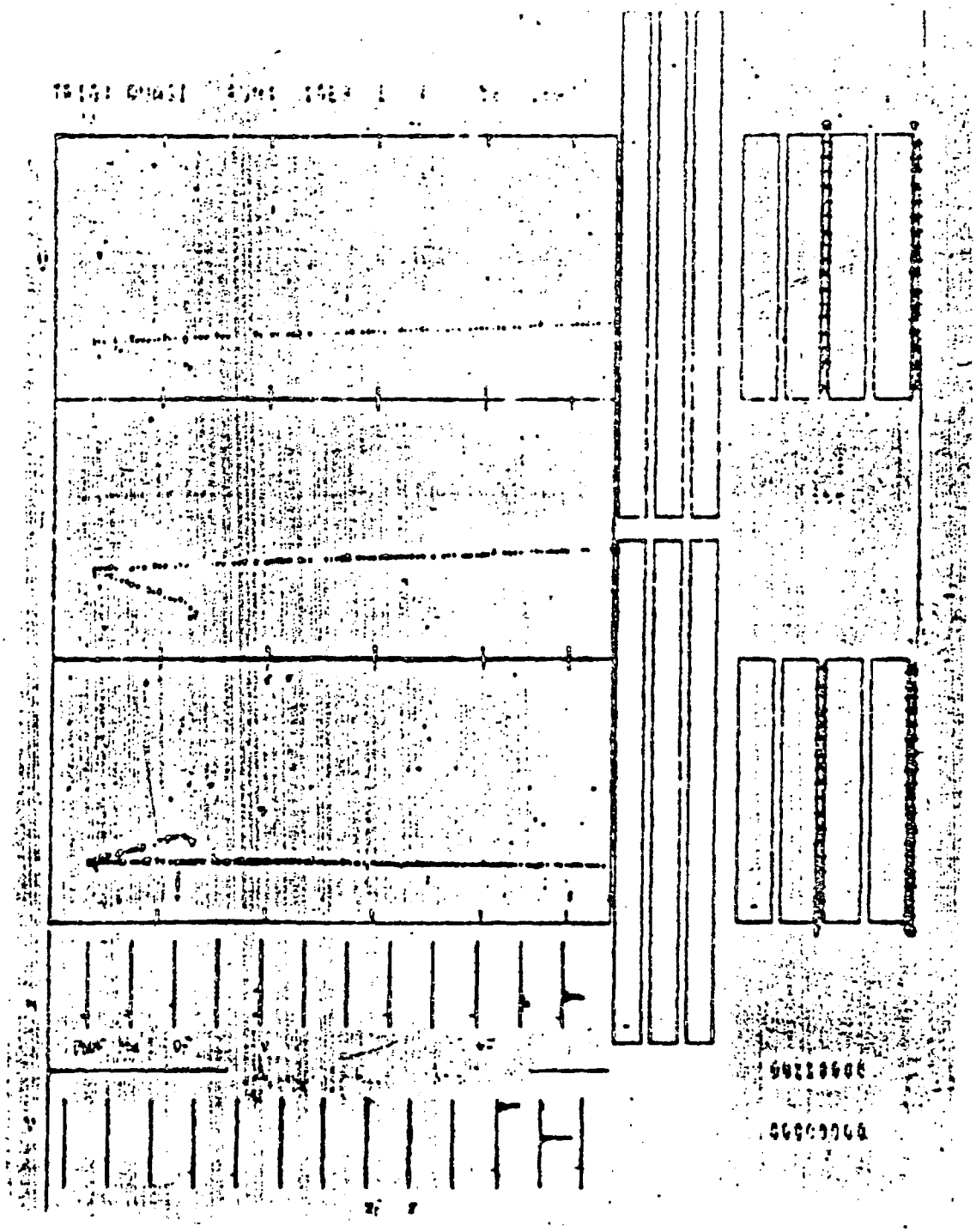

FIGURE 8a

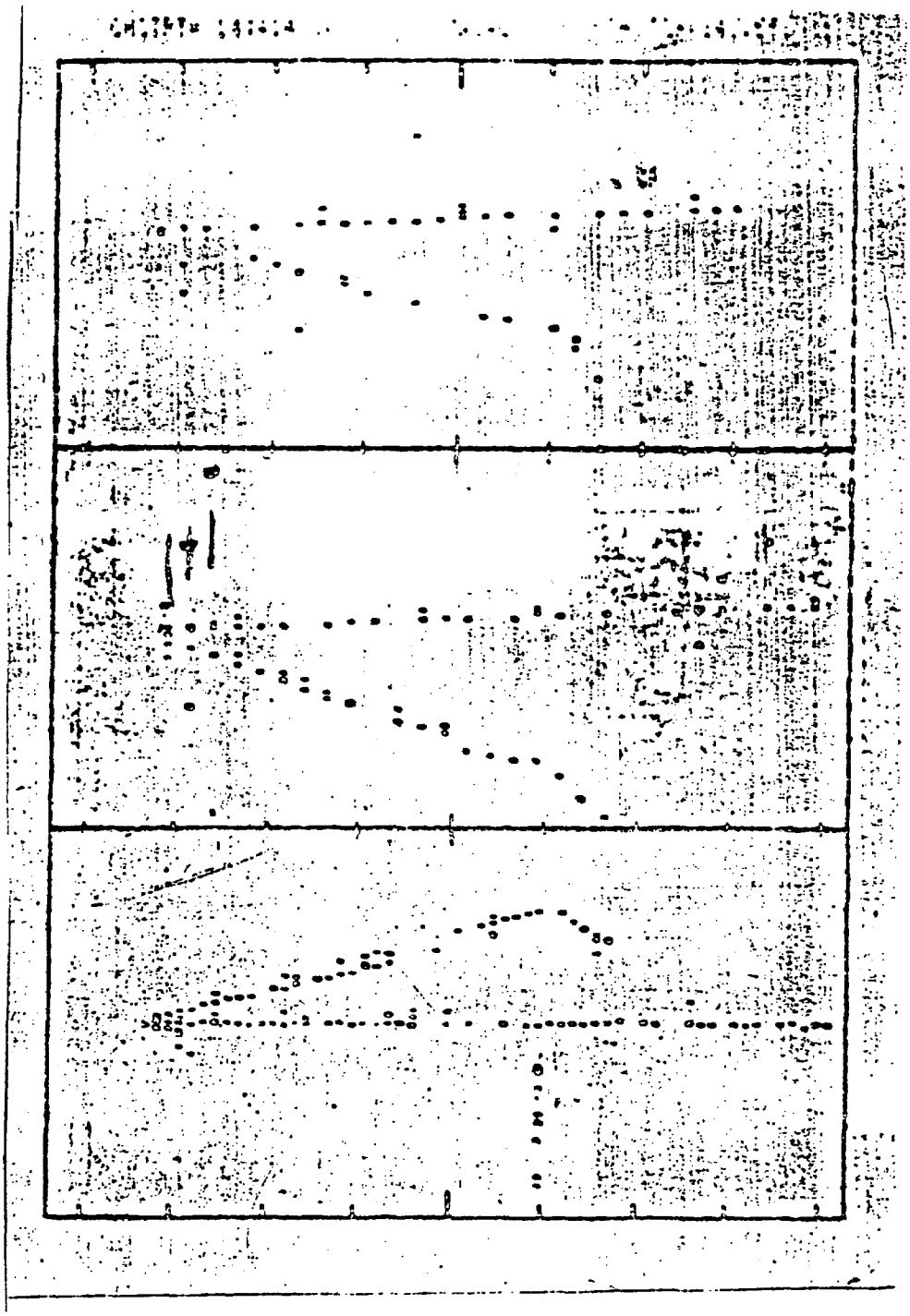

FIGURE 8b

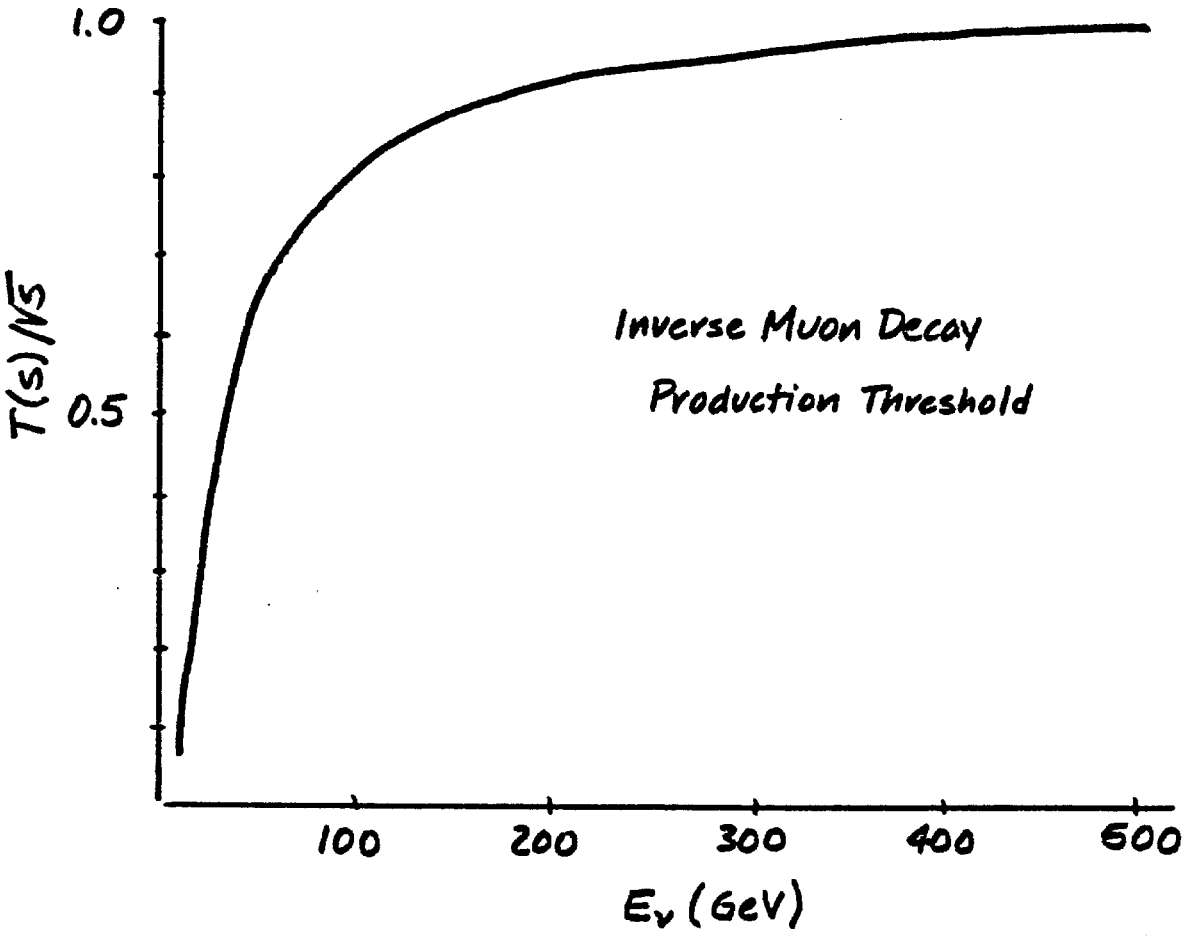
1.0
0.5
T(s)/NS
Inverse Muon Decay
Production Threshold
100
200
300
400
500
E_ν (GeV)

FIGURE 9

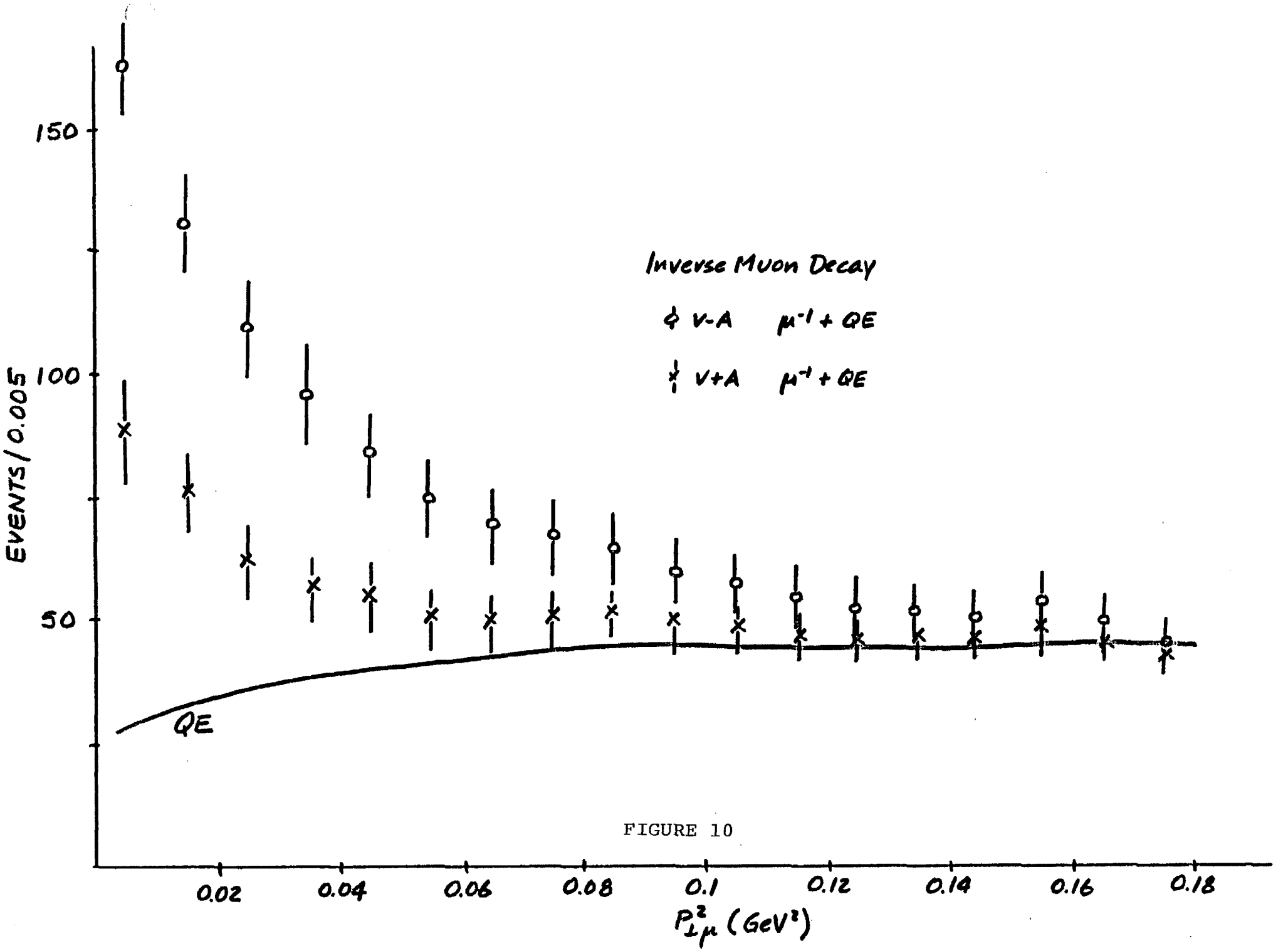
Inverse Muon Decay
V-A μ⁻¹ + QE
V+A μ⁻¹ + QE
QE
EVENTS/0.005
150
100
50
0.02
0.04
0.06
0.08
0.1
0.12
0.14
0.16
0.18
P²⊥μ (GeV²)

FIGURE 10

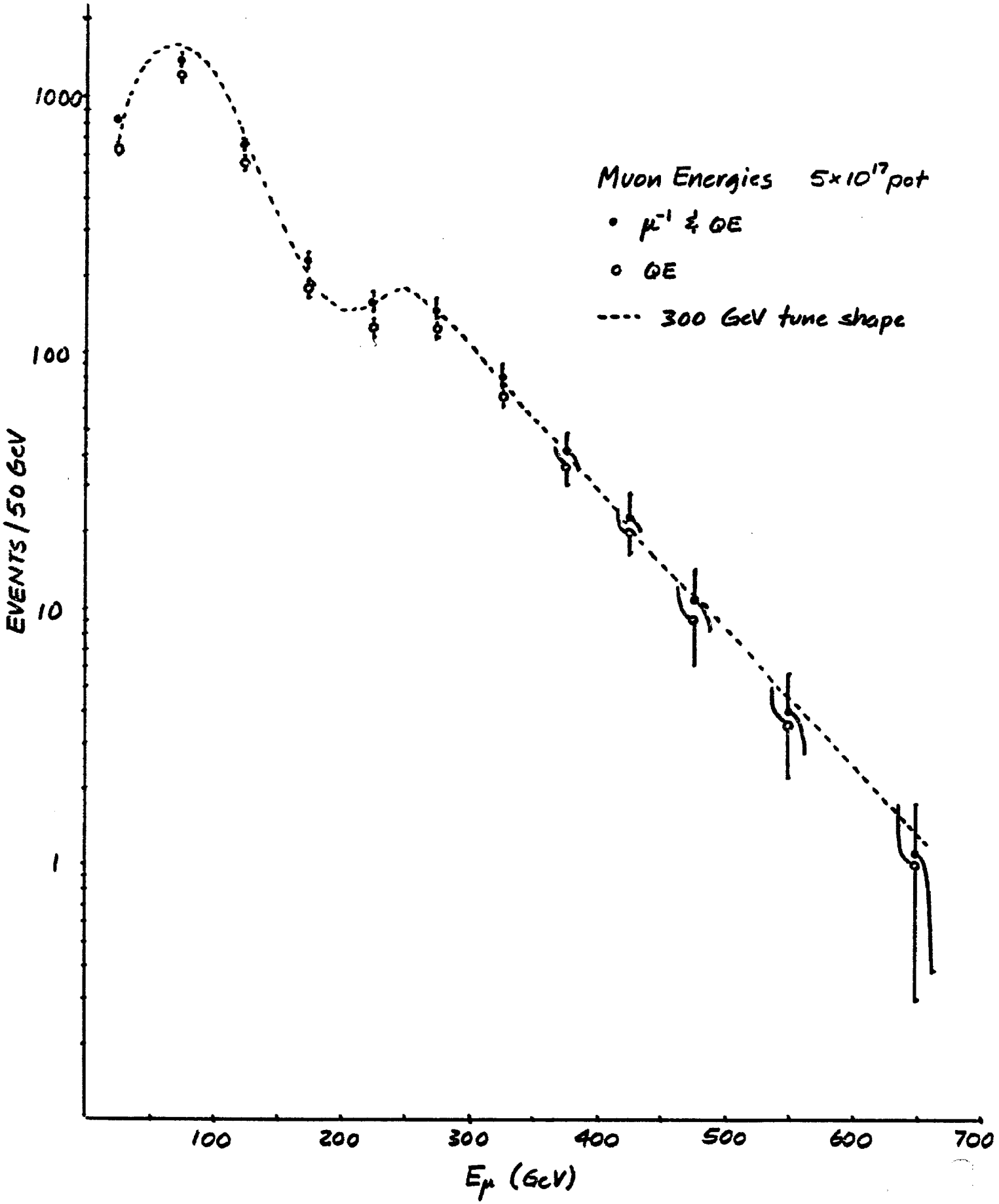
Muon Energies 5×10^17 pot
• μ⁻¹ & QE
o QE
---- 300 GeV tune shape
EVENTS / 50 GeV
1000
100
10
1
100
200
300
400
500
600
700
Eμ (GeV)

FIGURE 11

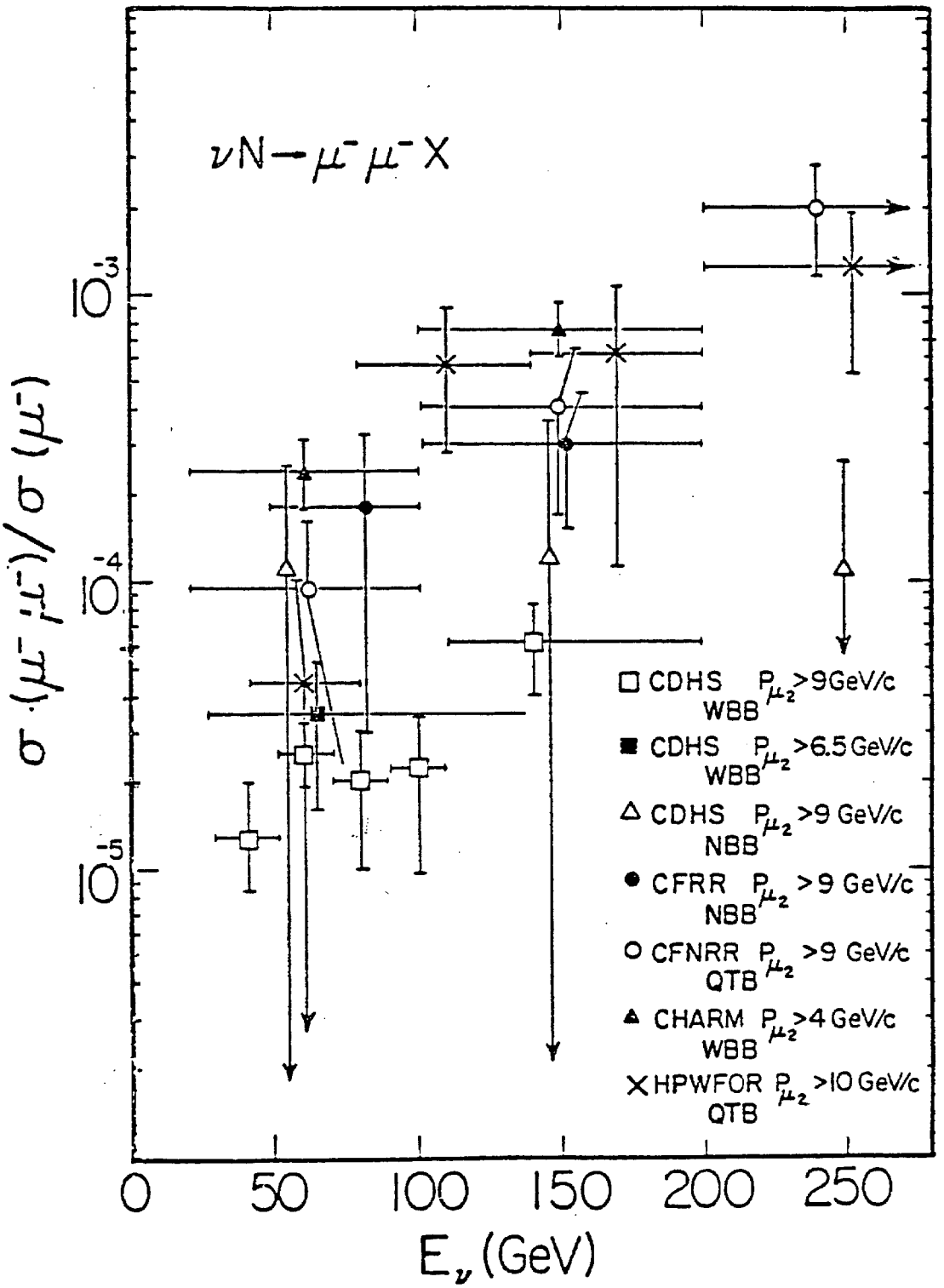
$\nu N \rightarrow \mu^- \mu^- X$
$\sigma \cdot (\mu^- \mu^-) / \sigma (\mu^-)$
10^{-3}
10^{-4}
10^{-5}
0
50
100
150
200
250
E_ν (GeV)
CDHS P_{μ_2} >9GeV/c WBB
CDHS P_{μ_2} >6.5 GeV/c WBB
CDHS P_{μ_2} >9 GeV/c NBB
CFRR P_{μ_2} >9 GeV/c NBB
CFNRR P_{μ_2} >9 GeV/c QTB
CHARM P_{μ_2} >4 GeV/c WBB
HPWFOR P_{μ_2} >10 GeV/c QTB

FIGURE 12

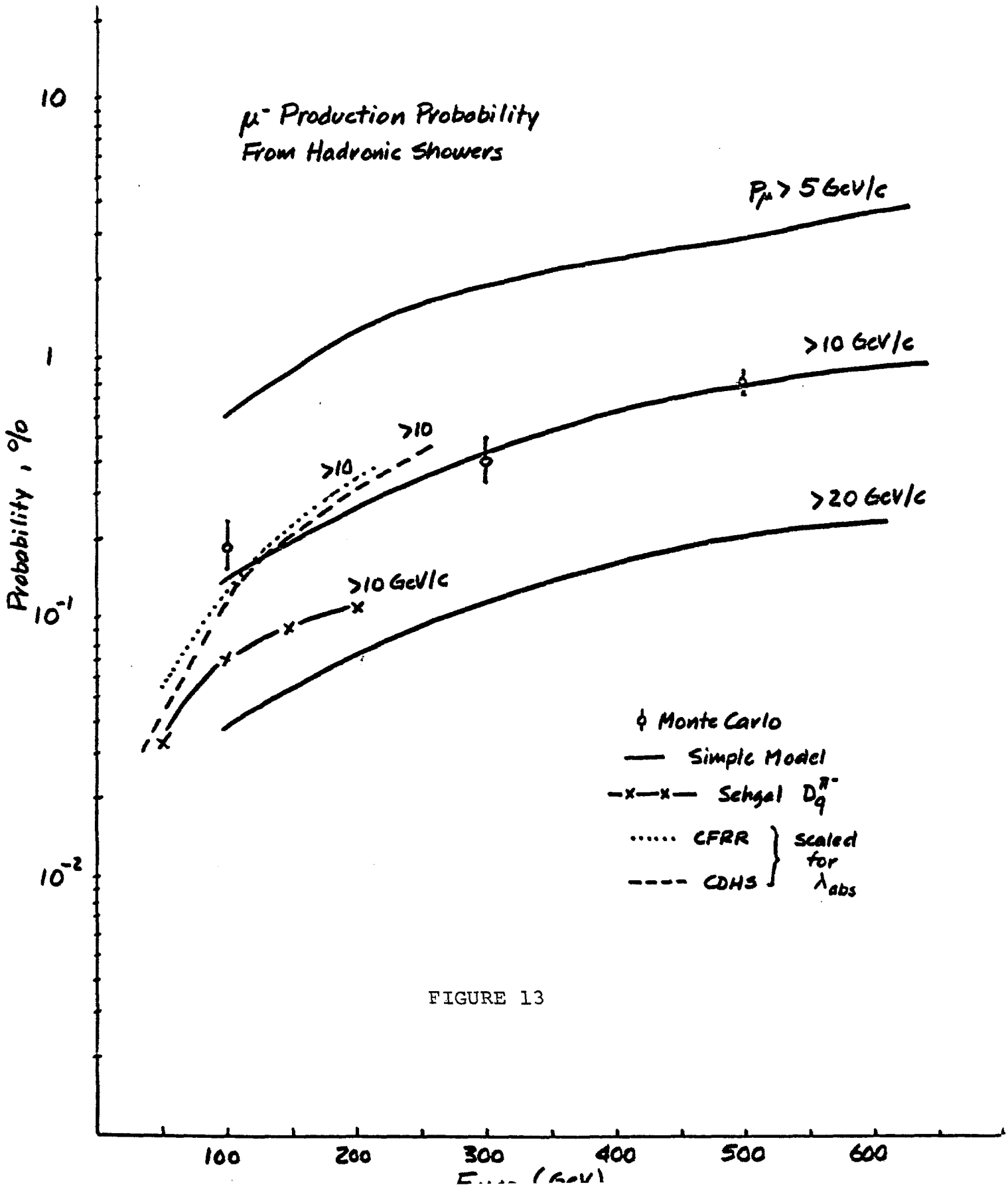
μ⁻ Production Probability
From Hadronic Showers
Probability , %
10
1
10⁻¹
10⁻²
Pμ > 5 GeV/c
>10 GeV/c
>20 GeV/c
>10
>10
>10 GeV/c
ϕ Monte Carlo
Simple Model
Sehgal $D_q^{\pi^-}$
CFRR
CDHS
scaled for λ_{abs}
100
200
300
400
500
600

FIGURE 13

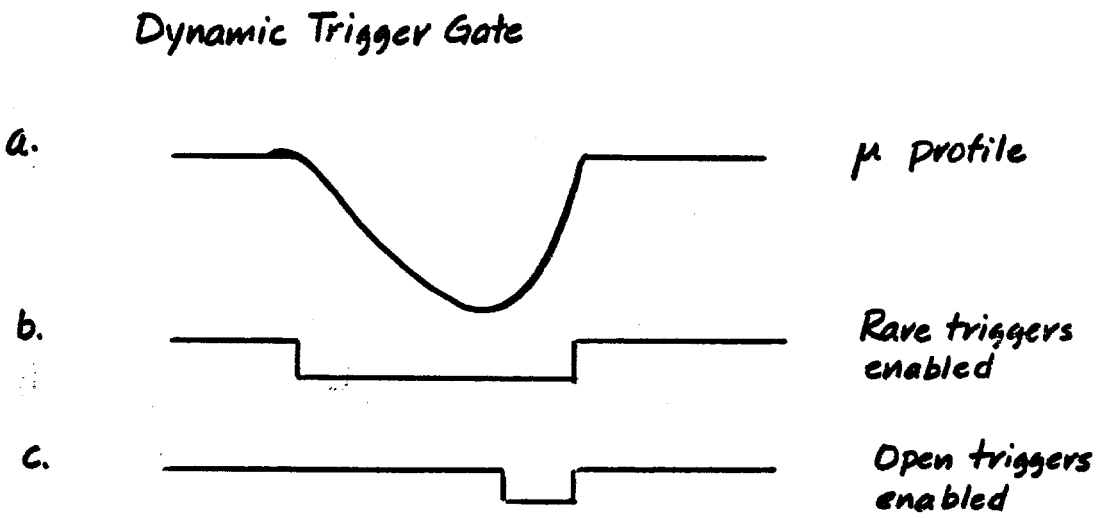
Dynamic Trigger Gate
a.
μ profile
b.
Rare triggers enabled
c.
Open triggers enabled

FIGURE 14

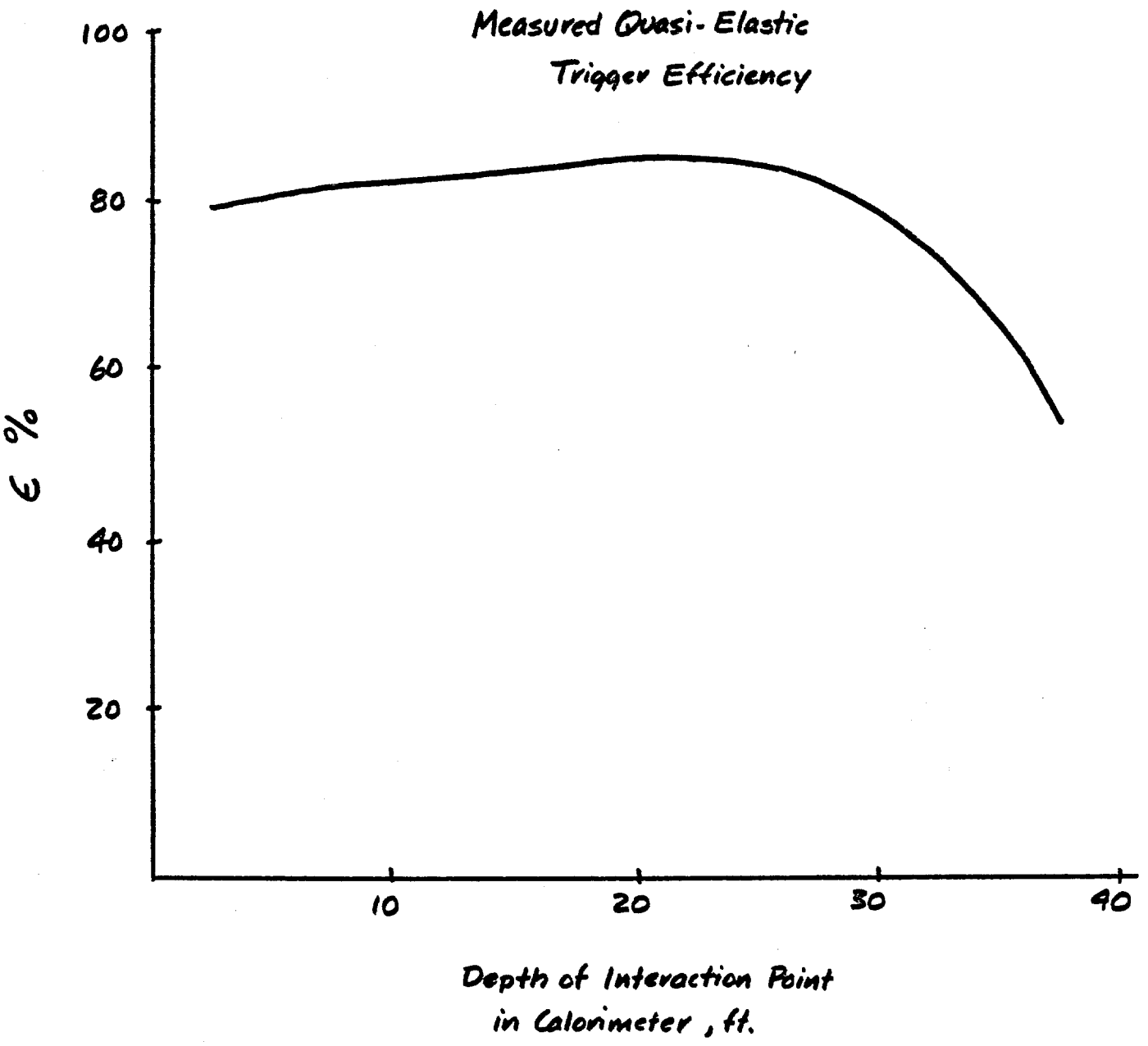
Measured Quasi-Elastic
Trigger Efficiency
100
80
60
40
20
ε %
10
20
30
40
Depth of Interaction Point
in Calorimeter, ft.

FIGURE 15

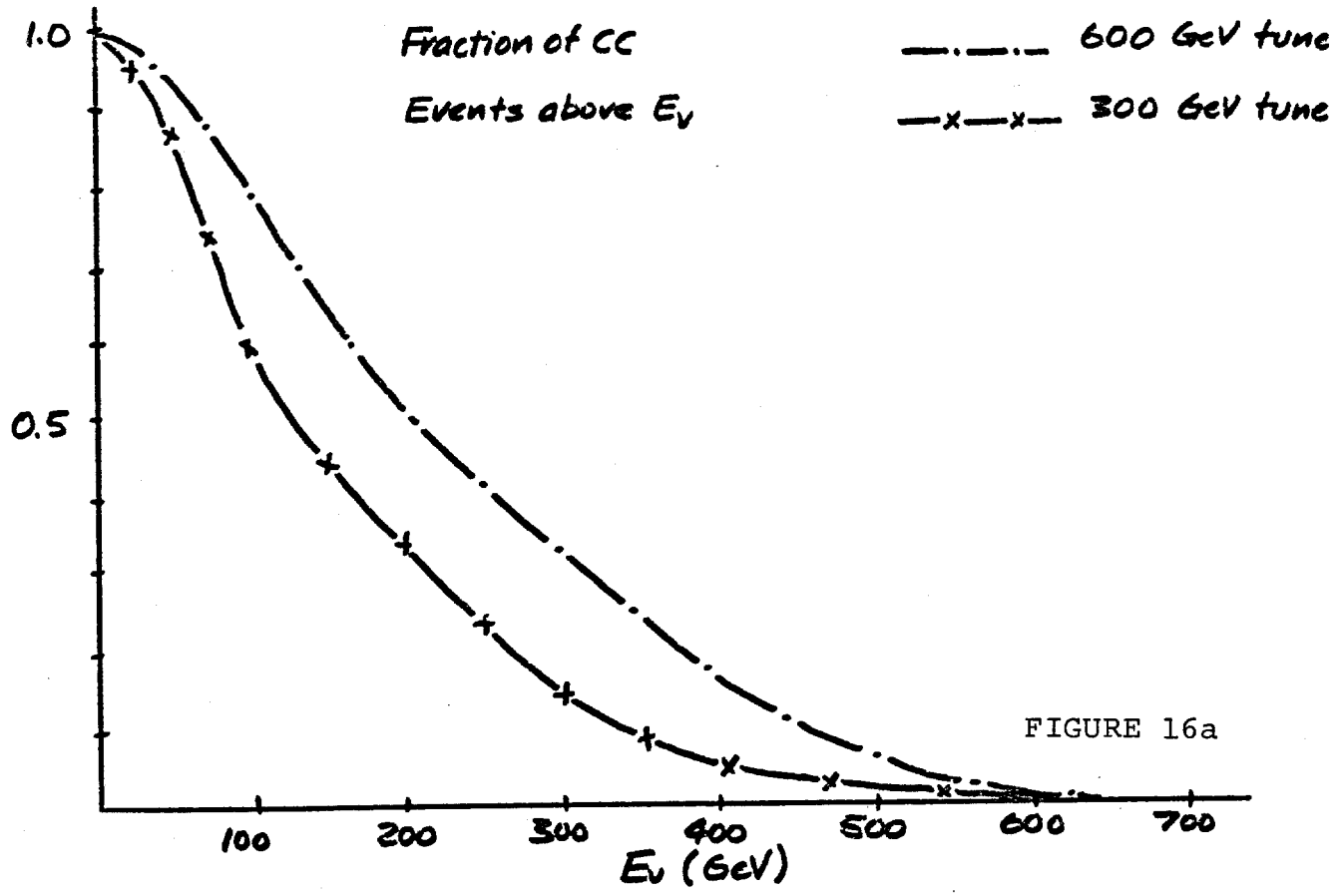

FIGURE 16a

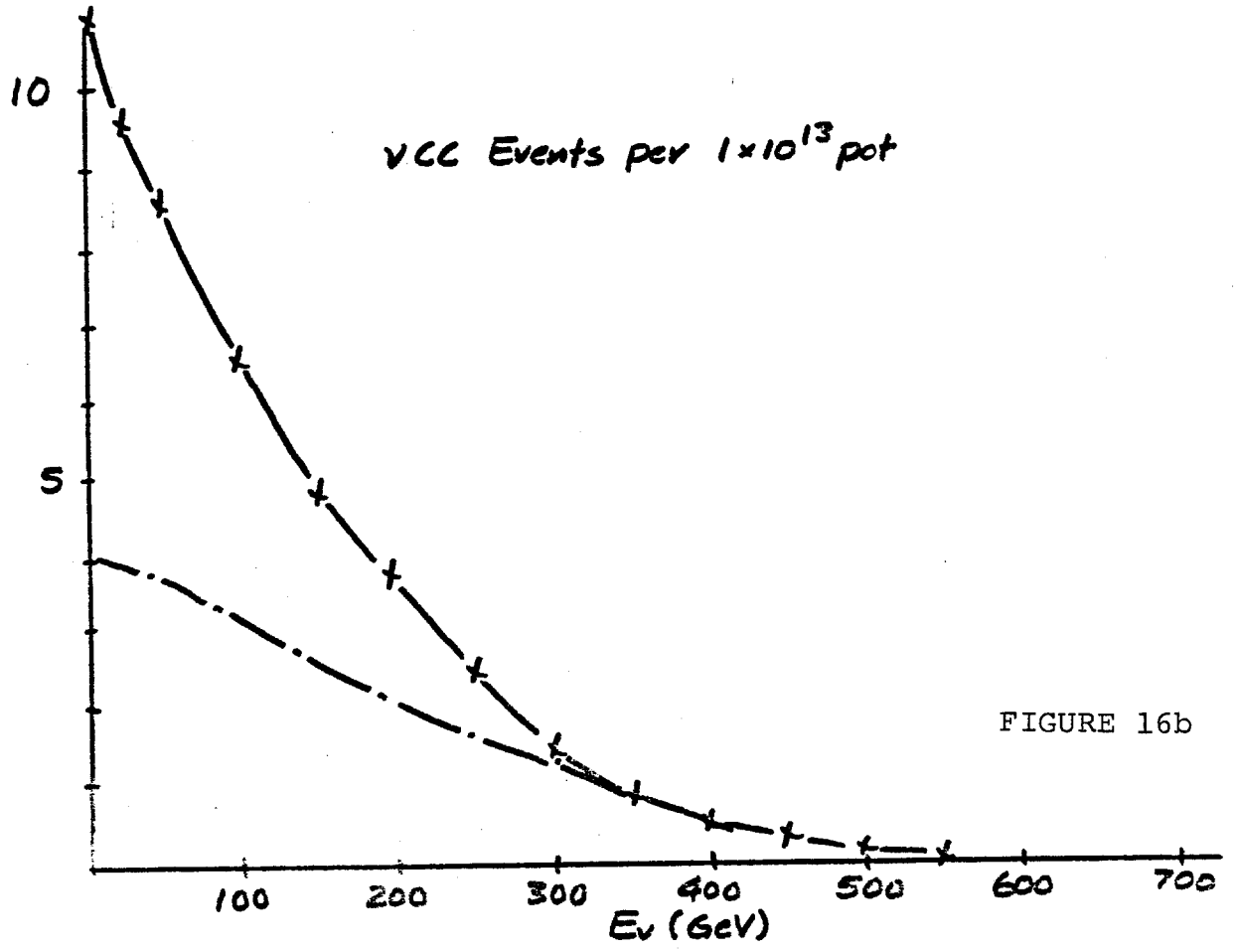

FIGURE 16b

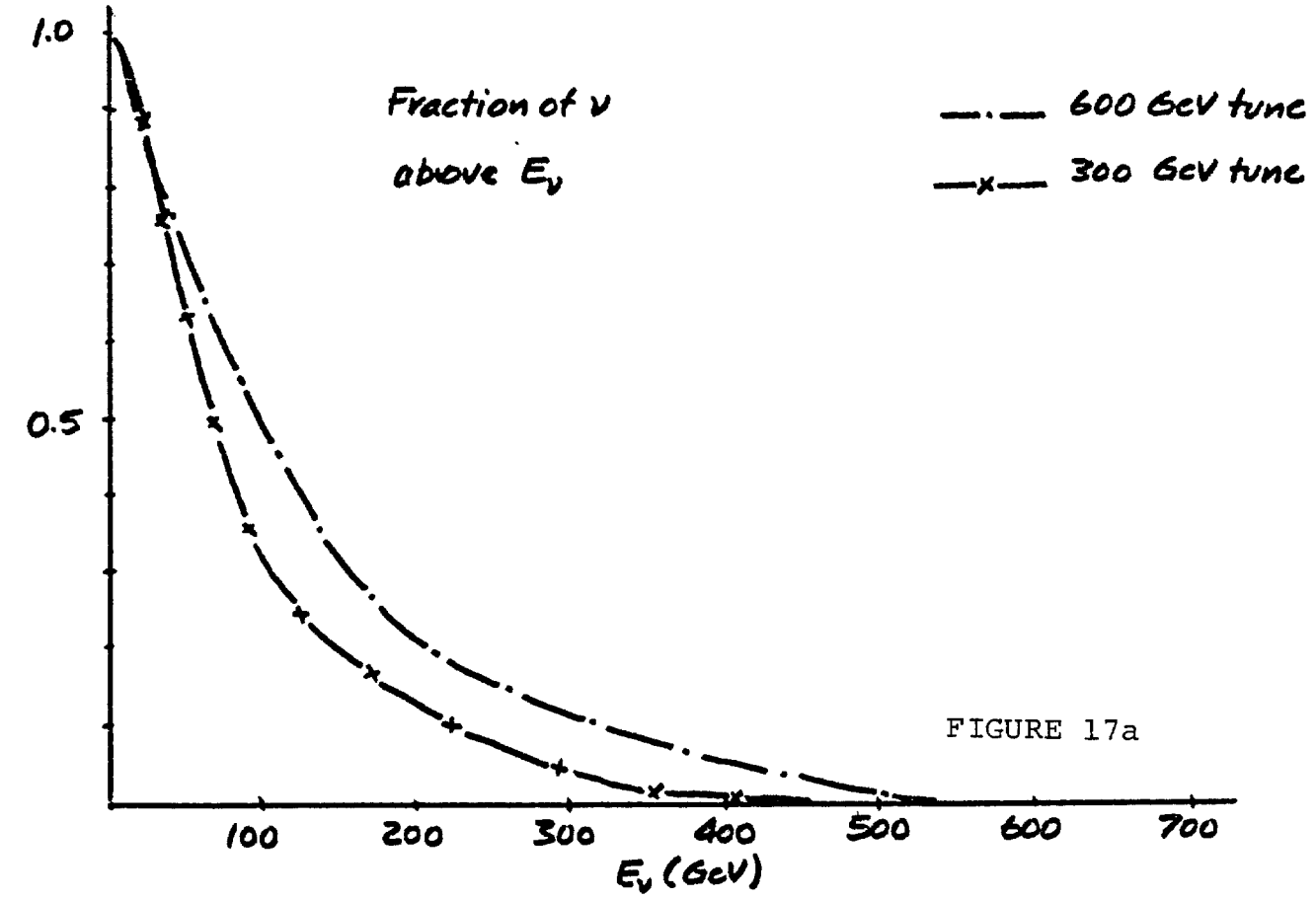

FIGURE 17a

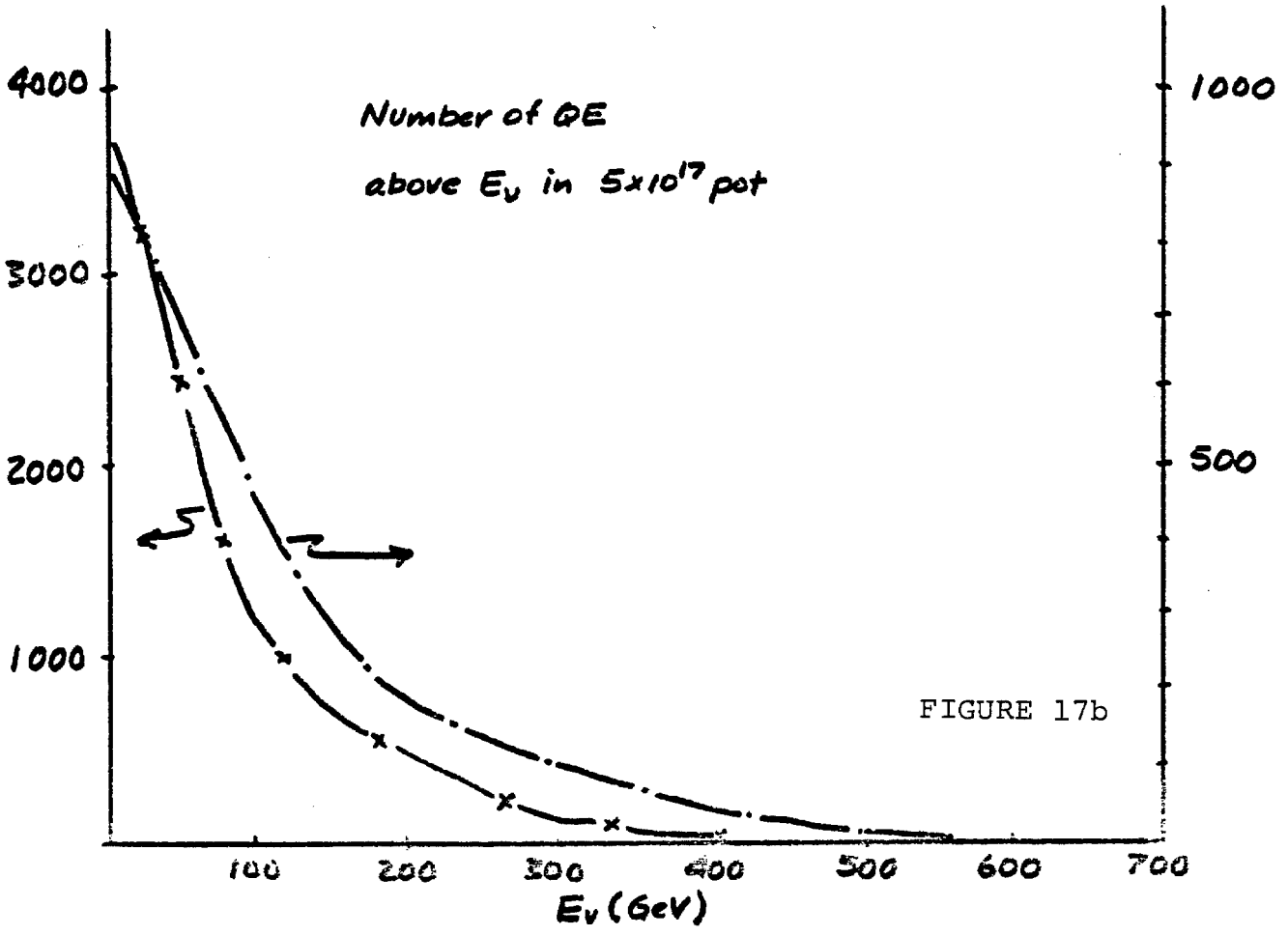

FIGURE 17b

VI. Appendices

A. The Apparatus

1. The Calorimeter

a. Arrangement of the Calorimeter

The Flash Chamber - Proportional Tube Calorimeter is 60 feet (18 meters) long comprising 340 metric tons (see Figure A1). The flash chambers are arranged in three views (X, Y and U) with cells which run 0^{o}, 80^{o} and 100^{o} relative to horizontal (see Figure A2). Each flash chamber is sandwiched by a sand plane and a steel shot plane. These target-absorber planes are made from extruded acrylic plastic sheets with 5/8" x 5/8" x 12' vertical cells filled with either sand or steel shot. Table AI shows the arrangment of the target-absorber planes within the flash chambers and lists the corresponding absorption and radiation lengths. The proportional tube planes are located one every 16 flash chambers. Hence, between adjacent proportional planes there are 0.5 absorption lengths (64 g/cm^2) or 3.5 radiation lengths. The proportional tubes are alternately vertical and horizontal.

b. General Properties

The average density of the calorimeter is 1.40 g/cm^3 and the average Z is 19.1. This low average Z was obtained by using sand as a part of the target-absorber and allowed us to measure the angle of electromagnetic showers. The average collision, absorption, and radiation lengths in the calorimeter are 51.8,83.1, and 11.7 cm respectively. The size of hadronic showers in the calorimeter, or more precisely the dimensions required for containment of the shower energy, is given in Figure A3 which are scaled from shower depth calculations in liquid scintillator by the HPWFOR group.[1] The hadronic shower resolutions, discussed below, demand that at least 99% of the shower is contained in the calorimeter longitudinally and at least 95% laterally. The calorimeter properties are summarized in Table AII.

c. The Flash Chambers

There are 608 flash chambers, each with approximately 650 5 mm x 5 mm cells. This fine granularity of the flash chambers allows a small sampling step of the recoil showers leading to excellent energy and angle determination, pattern recognition and muon track finding. The flash chambers are made of extruded black polypropylene with aluminum foil electrodes glued on both sides. Each flash chamber has an active area of 12' x 12' (3.66 m x 3.66 m). Standard spark chamber gas: 90% Ne, 10% He, plus some trace amounts of electronegative elements are circulated through the

cells.[2]

When an event is detected, a high voltage pulse of 4.25 kV is applied across each chamber for 0.5 μsec. During this high voltage pulse, a plasma discharge propagates down he full 12' length of the flash chamber cell and into a readout region at the end of each cell. A copper strip for each cell is glued over this 2-ft long readout region and develops a current pulse when the cell is hit. The current pulse is then read out by magnetostrictive techniques.

d. The Proportional Tubes

The trigger and energy determination at large energies are provided by planes of proportional tubes. There are 37 such planes, each containing 144 tubes. The planes are made of extruded aluminum. Each tube is 1" x 1" x 12' and is strung with a single 2 mil gold plated tunsten wire. Four tubes are connected to one amplifier to reduce the cost of electronics while still maintaining adequate granularity for versatile triggering purposes. An argon-methane (90%-10%) gas mixture is used to give fast drift times (200 ns) needed to form the trigger within the flash chamber sensitive time.

e. Scintillation Counters

Liquid scintillation counters with a 12' x 12' sensitive area are placed every 80 flash chambers throughout the calorimeter. The

most upstream counter will be an acrylic plastic wall instrumented with waveshifter bars and 12 phototubes and will serve as a front veto counter. The other scintillation counters will be used for efficiency measurements. Further, one more plastic plane is in the fifth toroid gap to provide timing information for the drift system.

f. The Muon Spectrometer

The muon momentum for charged current interactions and multi-muon events will be measured in the muon spectrometer at the rear of the apparatus (see Figure A1). There are three 24-ft diameter by 2-ft thick iron toroids immediately downstream of the calorimeter and four 12-ft diameter by 4-ft thick iron toroids behind these. The muons travel through 6.6 meters of magnetized iron at an average field of 18 kG, corresponding to a $p_\perp$ kick of about 2 GeV/c.

We have measured the magnetic field in each of the 24' and 12' toroid slabs. Each magnet was made from slabs of iron with small radial and non-radial slits into which a probe was inserted. Figure A4 shows the field as a function of radius for each slab with discontinuities showing at the slab boundaries. Figure A5 shows the measurement for each of the 12' magnets. There, the discontinuity is due to the non-radial nature of the slits.

g. Toroid Proportional Planes

In anticipation of the Tevatron era we are upgrading the position measuring system in the toroid proportional chambers. At low muon energies (~100 GeV), the multiple scattering in the iron toroids gave transverse position uncertainty comparable to the widths of the proportional tubes themselves (~1 cm). Simply measuring which tube was traversed gave as good a momentum accuracy as possible. At Tevatron energies (approximtely 600 GeV) this is no longer the case: multiple scattering is in the millimeter range.

We are building a system which will measure the drift time within each proportional tube which will act as a vernier in position measurement. The drift time is measured by clocking the pulse arrival with respect to a common stop provided by a plastic scintillator plane. The clock time is chosen so that we can bin the particle position in units of 1 mm. Within this accuracy, we expect to be able to measure muon momenta to a precision of 8 to 20% (see Figure A9).

Prototype electronics have been built and tested by measuring the errors in a straight line fit to cosmic rays through an eight tube system. The measured error was consistent with that expected from time bins of 20 ns. The schedule calls for testing the system in planes this spring and installation in Lab C during the fall of 1983.

h. Proportional Plane Triggering

Each of the 36 4 wire channels of each calorimeter proportional plane is capable of generating a fast, differential analog output pulse (FO). The fast processing electronics on each plane discriminates these 36 FO signals with respect to a preprogramed threshold (typically, 20 mV). These discriminated FO signals (DFO) are then combined to generate several analog and logic signals used in an event trigger:

1. Sumout (Σ_i): This signal is the linear sum of the undiscriminated individual FO signals from plane i making a single analog pulse for each plane which is proportional to energy deposition.

2. Analog Multiplicity (AM_i): This is an analog signal with a pulse height proportional to the number of DFO signals in plane i and so is a measure of the shower width.

3. Single (S_i): This output is the logical "OR" of all the DFO in plane i. This signal has served in the past as an efficient veto for muons (80%).

4. Fat Shower Veto (FSV_i): This output is a logic pulse generated when the ionization pattern width in plane i is determined to have exceeded a programed width (a multiple of 4" segments).

5. SumSum ($\Sigma\Sigma$): This signal is the sum of all Σ_i in the calorimeter, a measure of the total energy deposited in a shower.

6. Multiplicity (M): This signal is generated if the number of Σ_i is greater than (or less than) some preset number specified by the trigger criteria. This signal can function as a shower length

requirement.

7. Toroid multiplicity (TM_i): This signal is similar to AM_i in the calorimeter, specifying the number of tubes in the ith toroid plane which had a pulse height above a preset amount. This will be a feature of the new drift chamber system.

8. Muon straightness (MS): This yes-no requirement signifies that a muon is straight within a road of the 8" channel widths in the entire toroid system. The minimum momentum corresponds to roughly 30 GeV/c and the trigger would have an efficiency shown in Figure A6 reaching 100% by 200 GeV/c.

2. Resolutions

a. Energy Resolution

The hadronic shower energy is measured by cell counting using the flash chambers at low energies and pulse height using the proportional tubes at high energies (see Figure A7). Because of their fine grained sampling, the flash chambers provide good resolution as low as 10 GeV. At high energies (above ~200 GeV), where saturation becomes relevant, the proportional tubes provide a good energy measurement.

The flash chmaber energy resolutions in Figures A7 were directly measured in hadron and electron beams on two previous runs. The proportional tube resolution Figure A7 was estimated by scaling

Anderson et al.[3]

b. Angular Resolution

The hadronic shower angular resolution determined by the calorimeter is also shown in Figure A7. The angular resolution depends critically on the spatial resolution of the shower vertex. The angle of the showers is computed by first locating the vertex and then using the "center of gravity" of the shower as a function of shower depth.

c. Pattern Recognition

As shown previously, we are able to distinguish electromagnetic from hadronic showers by their size, shape and structure. This was an important capability for the study of ν-e scattering where hadronic backgrounds are large. Furthermore, the fine granularity makes it possible for us to distinguish inelastic from elastic ν_μ interactions (important in the reaction $\nu_\mu n \rightarrow \mu^- p$ and $\nu_\mu e \rightarrow \nu_\mu e$). Figure A8 shows examples of data and Monte Carlo generated events of particularly interesting topologies.

We will also be able to observe, and locate the muon track in charged current interactions with some ability to point it back to the vertex. We expect a very small number of charged current interactions posing as neutral current interctions as a result of an escaping muon, especially at high energies.

d. Muon Momentum Resolution

Figure A9 shows the muon momentum resolution we expect to achieve when the 24 and 12-ft iron torids are instrumented with drift tubes. The drift tubes will provide position measurements with an estimated σ of 1 mm. As is done presently, the flash chambers will supply information regarding the muon's trajectory at the point of entry into the first toroid. The resolutions corresponding to the drift tube and flash chamber position measurements, as well as multiple scattering were used to produce the resolution shown.

B. Performance of the Calorimeter

1. Flash Chamber Performance

We have debugged and operated 608 flash chambers in the dichromatic exposure, E594 and we find that the flash chambers have performed well.[2] Using cosmic ray muons between neutrino triggers we have measured and monitored over long periods their efficiency at the proportional tube trigger time delay (650 ns from the event to the time high voltage appears across the chambers) to be between 70 and 80%. The multiplicity (cells lit per flash chamber per cosmic ray) is about 1.3. Adequate recirculation of the neon-helium gas was found to be 1.5% of the volume per minute which for the entire detector implies a recirculation rate of 900 liters per minute. The high voltage plateau region is broad: 3.5 to 5.5 kV (see Figure B1) and the signal-to-noise ratio of the amplified signals on the magnetostrictive lines is 10:1. A reasonable repetition rate with a few percent cell reignition thus far is ~1 flash per approximately 5 seconds. This is achieved by adding trace amounts of Argon and electronegative gases and lowering the high voltage 250 V from the earliest running in 1980.

2. Proportional Tube Performance

The proportional tubes have also performed well.[2] Using 90% argon - 10% methane gas and running at a high voltage of 1650 volts

gives us a gas gain of about 3000 and drift times of 200 ns. The amplifier gain is 1 mV/fC. A minimum ionizing particle gives a signal of 8 mV: a factor of 8 above noise. The linear swing is 0-2 volts or 0-500 particles. This is a factor of 2 or so above the largest number of particles per channel expected for Tevatron energy showers. The tube to tube uniformity has been measured to be very good: a plot of CA^{109} peaks for a large sample of tubes shows a σ of 5%.

Appendices A and B

Footnotes

[1]F. J. Sciulli, Proceedings of the Calorimeter Workshop, Fermilab, 79 (1975).

[2]D. Bogert et al., The Operation of a Large Flash Chamber Detector at Fermilab, Proceedings of IEEE Transactions on Nuclear Science NS 29, 363 (1982).

[3]R. L. Anderson et al., IEEE Transactions on Nuclear Science NS 25, 340 (1978).

Appendix A

Table Captions

AI Arrangement of Calorimeter Components.

AII General Properties.

Tonnage:	340 metric tons
Fiducial Tonnage for a Neutral Current Experiment:	100 metric tons
Fiducial Tonnage for a ν-e Scattering Experiment:	225 metric tons
Average Density:	1.40 g/cm^3
Average Z:	19.1
Average λ_{COL}:	51.8 cm
λ_{ABS}:	83.1 cm
X_o:	11.7 cm

TABLE AI

flash chambers:	U		X		Y		X	. . .
		↑		↑		↑		↑
absorber planes:		shot		sand		shot		sand
absorption lengths:		3.7%		2.5%	}	6.1% per view ($7.2\ g/cm^2$)		
radiation lengths:		36%		8%	}	44% per view		

TABLE AII

Appendices A and B

Figure Captions

A1 Plan view of detector

A2 Arrangement of the Flash Chambers

A3a Length of calorimeter required to contain 99% (or 90%) of the length of a shower.

A3b Radius of calorimeter required to contain 99% (or 95%) of a shower.

A4 Magnetic field strength measured for all 24' toroid slabs. Irregularities appear to be due to magnet construction. Calculations suggest that these irregularities affect the magnetic field only near the gaps.

A5 Magnetic field strength measured for all 12' toroid slabs.

A6 Trigger efficiency for muon straightness criterion within an 8" road.

A7 Angular resolutions for a) electrons and muons c) hadrons and energy resolutions for b) electrons and d) hadrons. The dashed curve is the energy resolution expected for the proportional tubes.

A8 Event displays for: a)-d) Monte Carlo—generated neutrino charged current events e)-f) deep inelastic data g)-i) unusual topologies seen in previous running.

Appendices A and B

Figure Captions

A9 Muon momentum resolution for drift tube-instrumented toroids.

B1 Flash Chamber high voltage plateau. Running conditions refer to the open circle curve for 4.25 kV on the chamber.

E-594 NEUTRINO DETECTOR

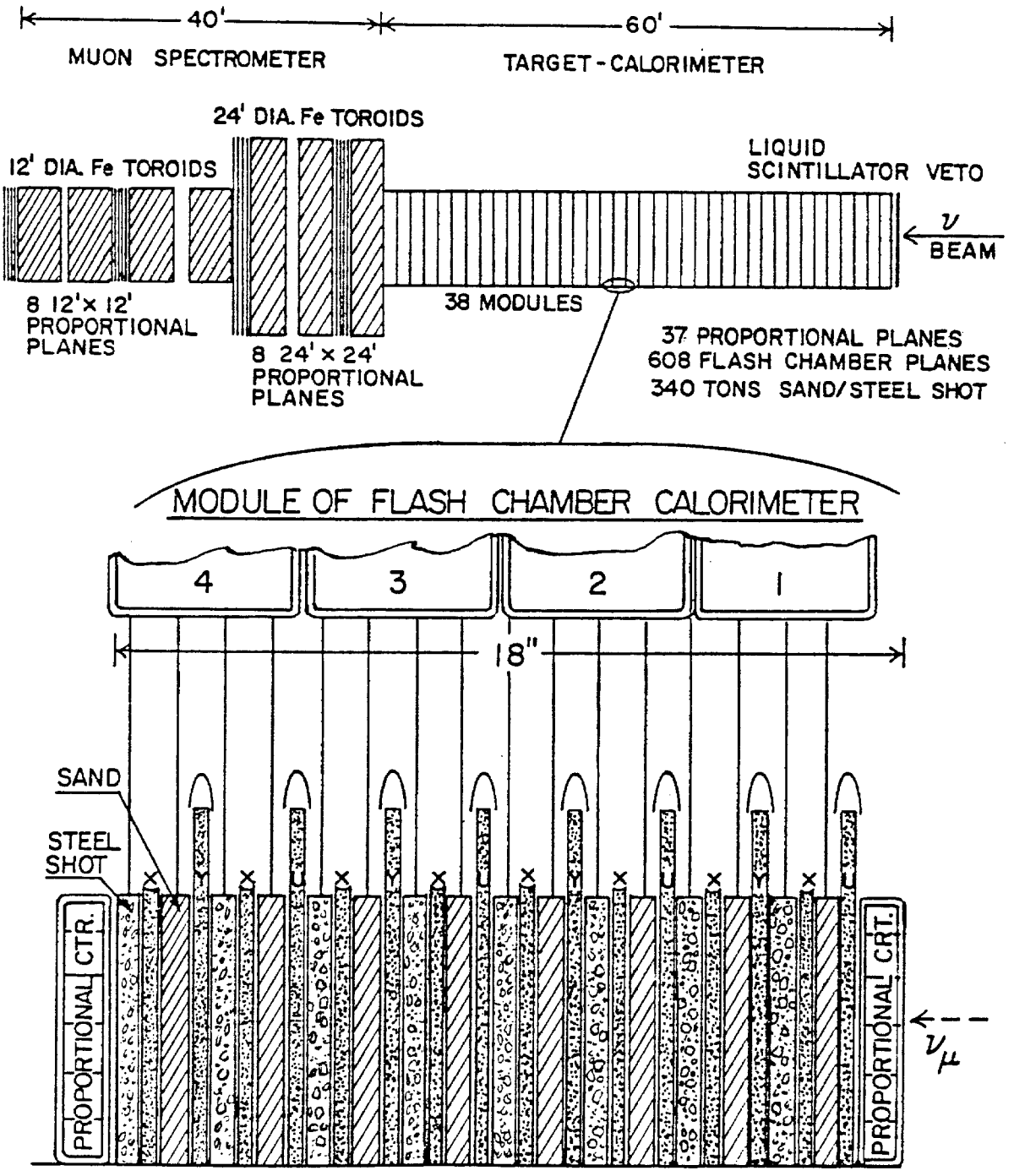

FIGURE A1

FLASH CHAMBER CALORIMETER CONSTRUCTION

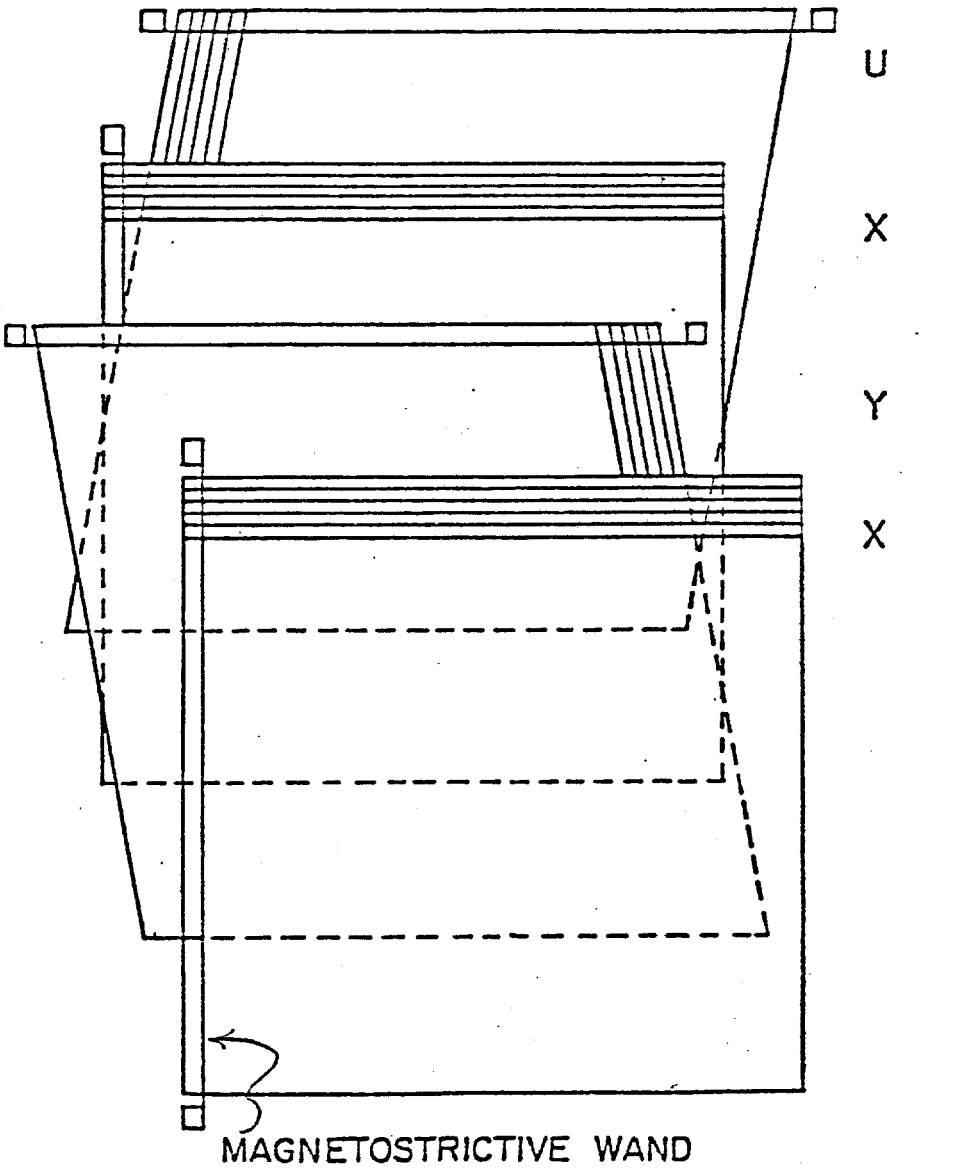

FIGURE A2

FIGURE A3a

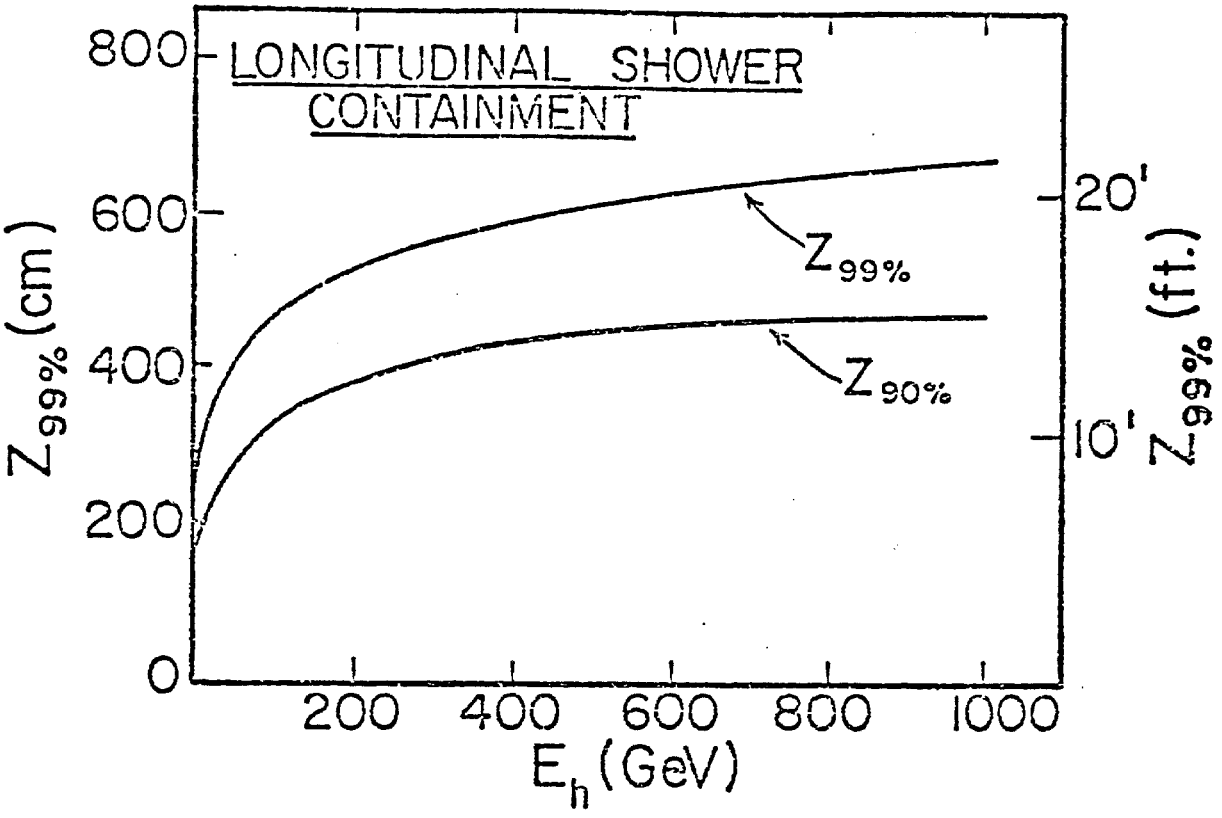

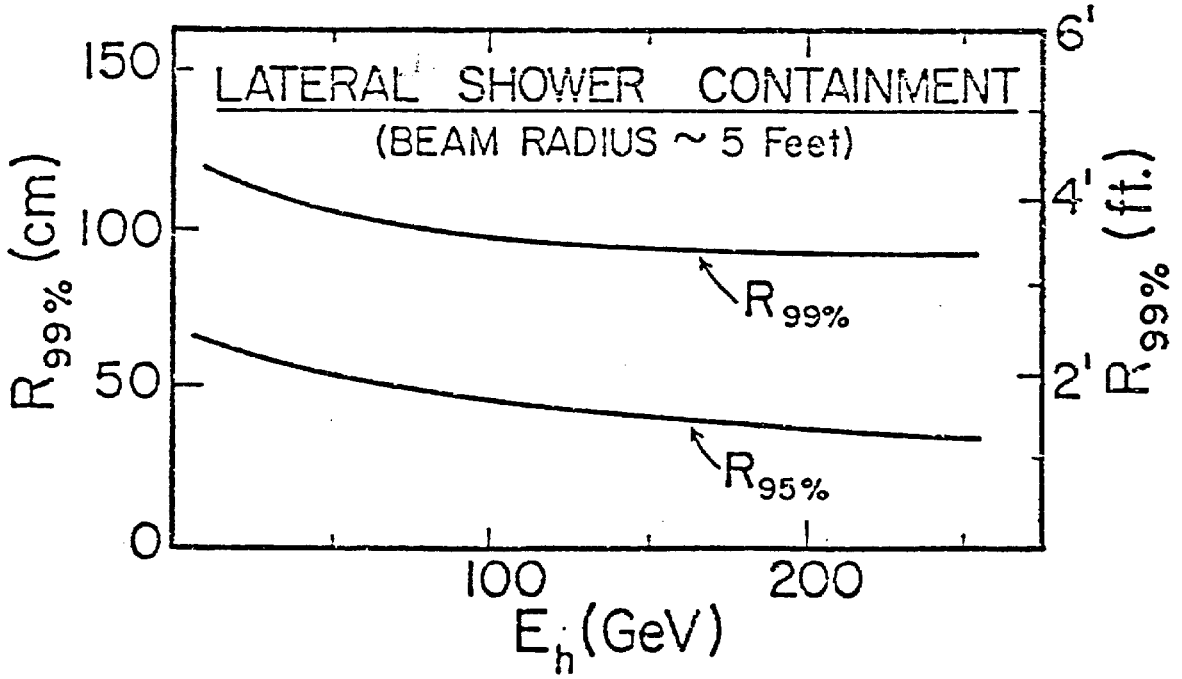

FIGURE A3b

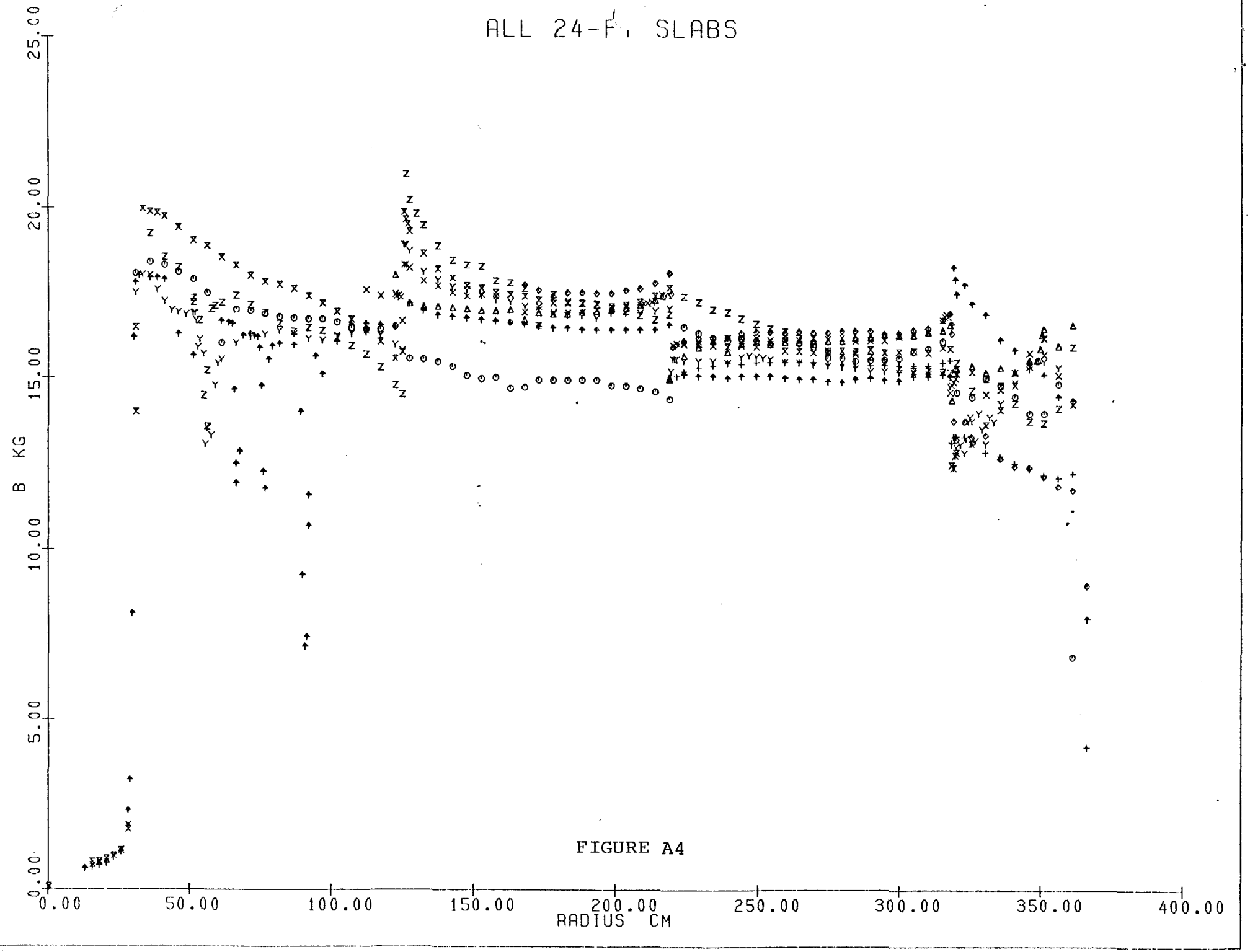
ALL 24-F, SLABS
B KG
25.00
20.00
15.00
10.00
5.00
0.00
0.00
50.00
100.00
150.00
200.00
250.00
300.00
350.00
400.00
RADIUS CM

FIGURE A4

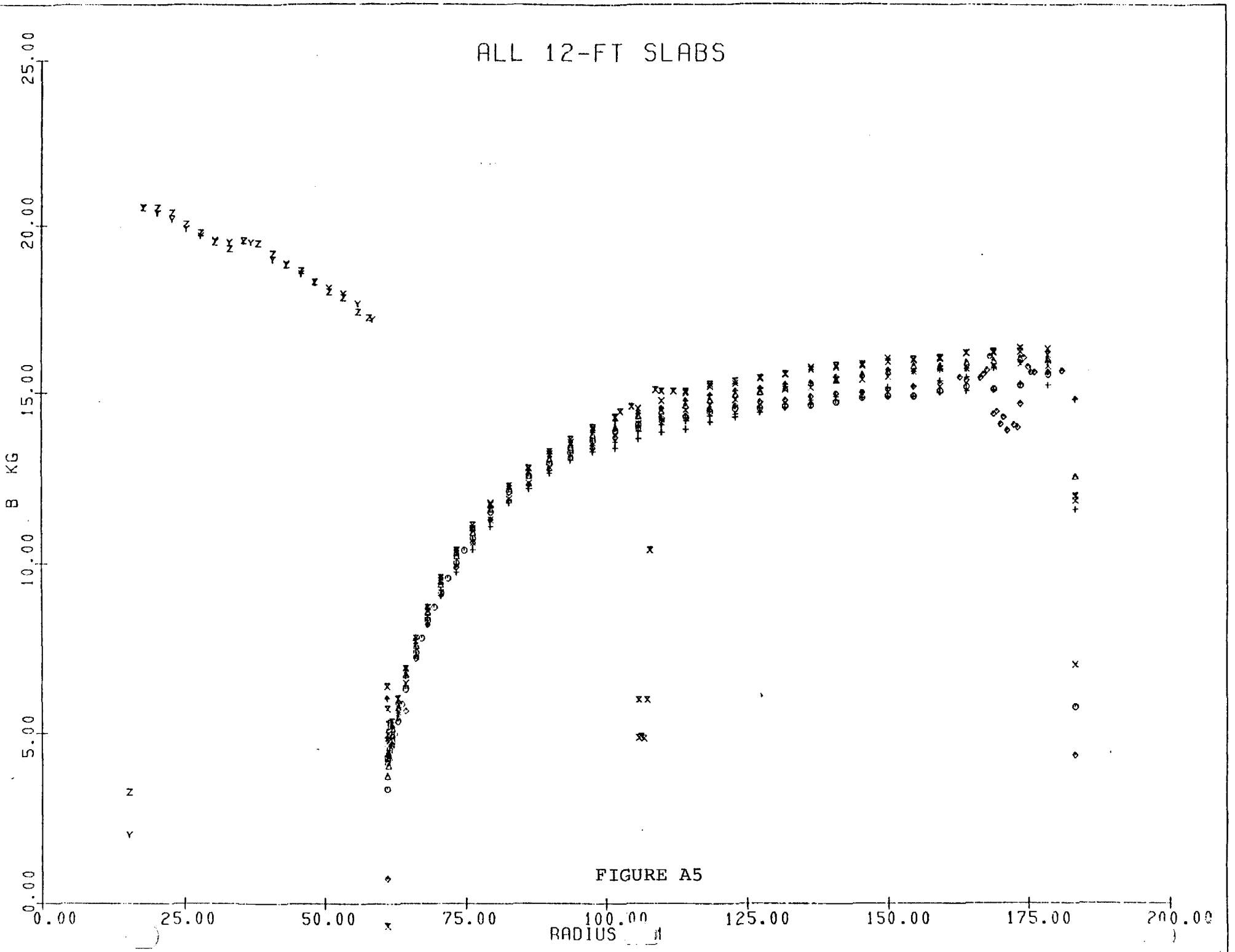
ALL 12-FT SLABS
B KG
25.00
20.00
15.00
10.00
5.00
0.00
0.00
25.00
50.00
75.00
100.00
125.00
150.00
175.00
200.00
RADIUS

FIGURE A5

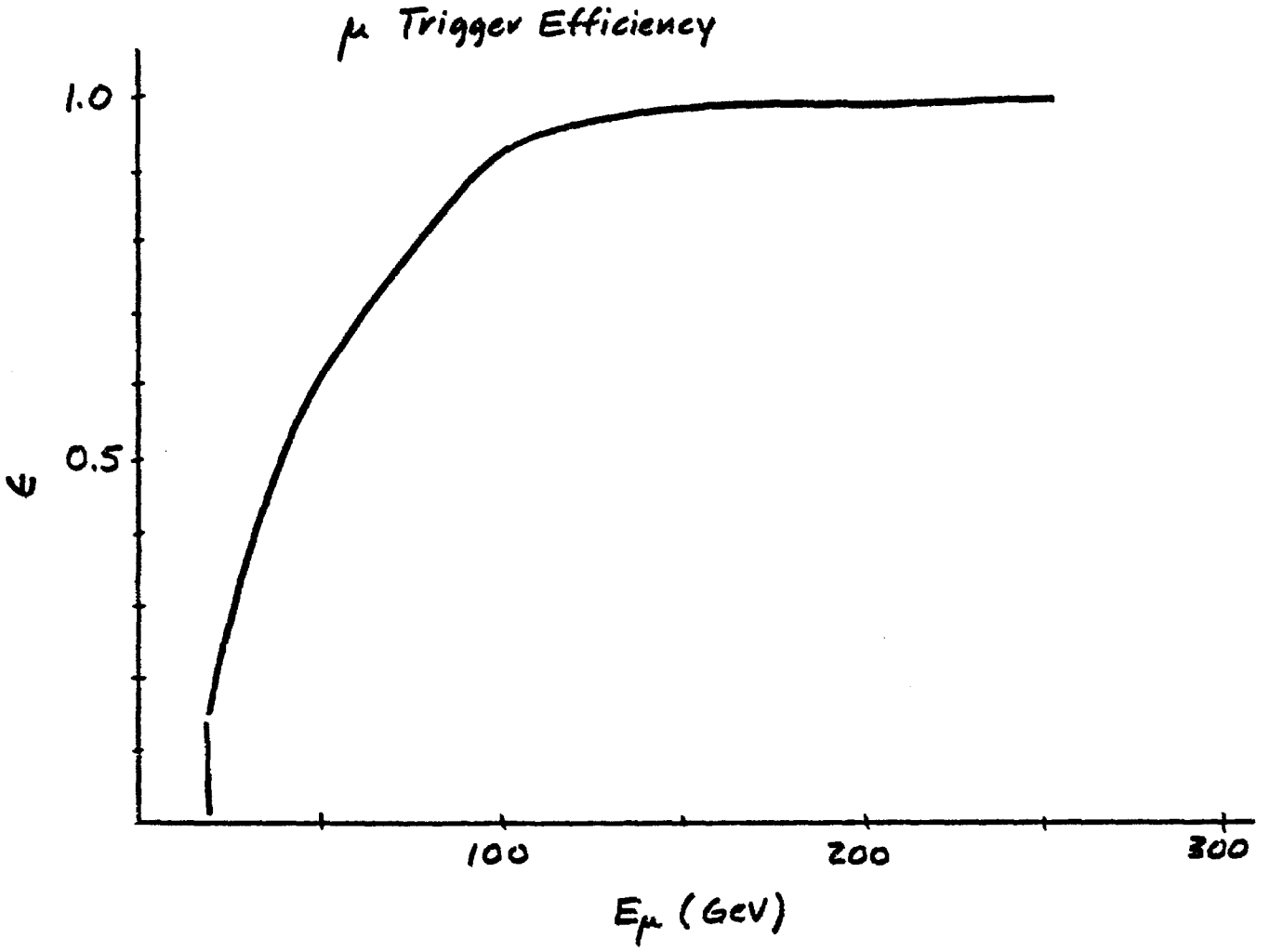

FIGURE A6

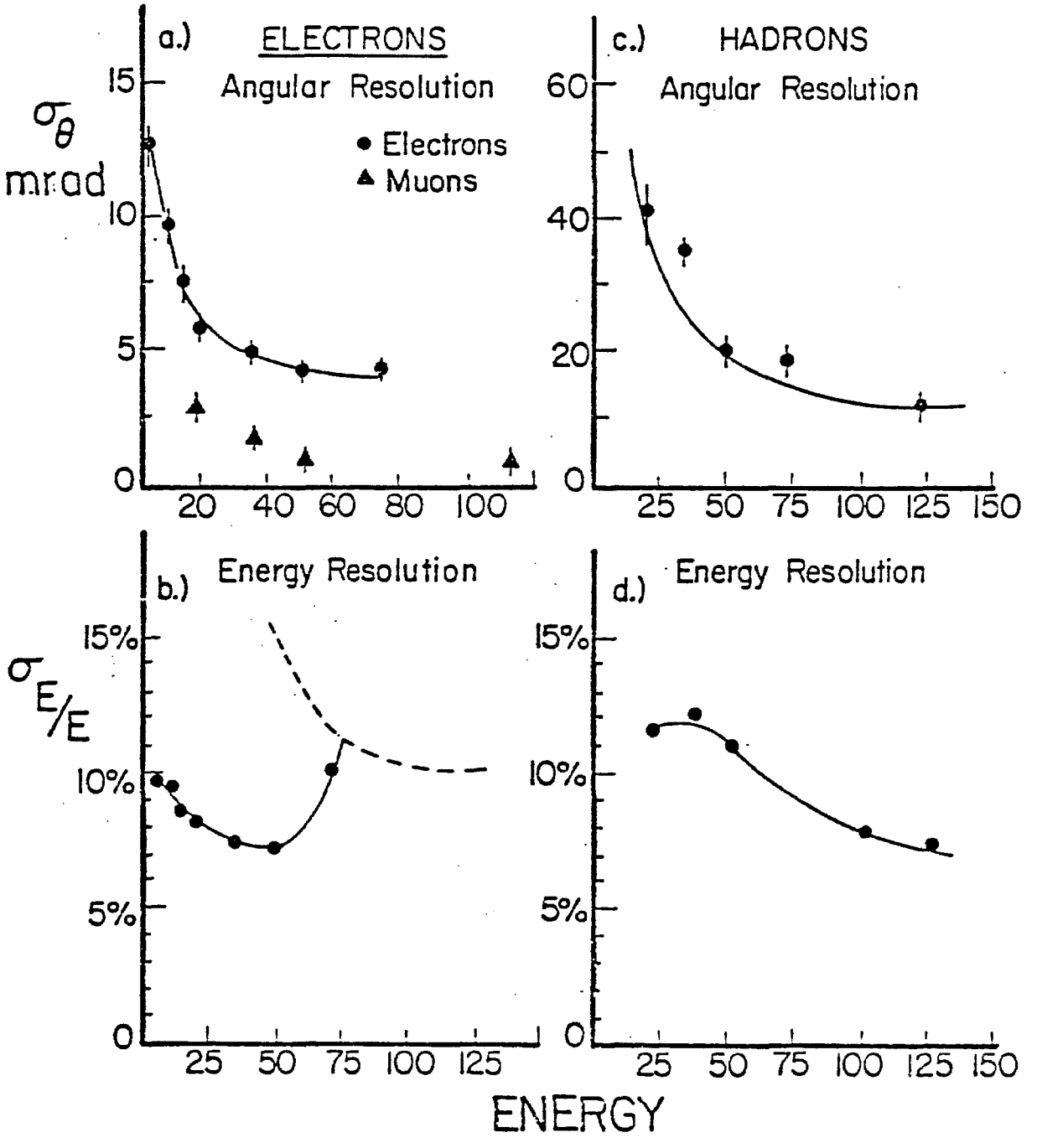
a.) ELECTRONS
Angular Resolution
σ_θ m.rad
Electrons
Muons
15
10
5
0
20 40 60 80 100
c.) HADRONS
Angular Resolution
60
40
20
0
25 50 75 100 125 150
b.) Energy Resolution
$\sigma_{E/E}$
15%
10%
5%
0
25 50 75 100 125
d.) Energy Resolution
15%
10%
5%
0
25 50 75 100 125 150
ENERGY

FIGURE A7

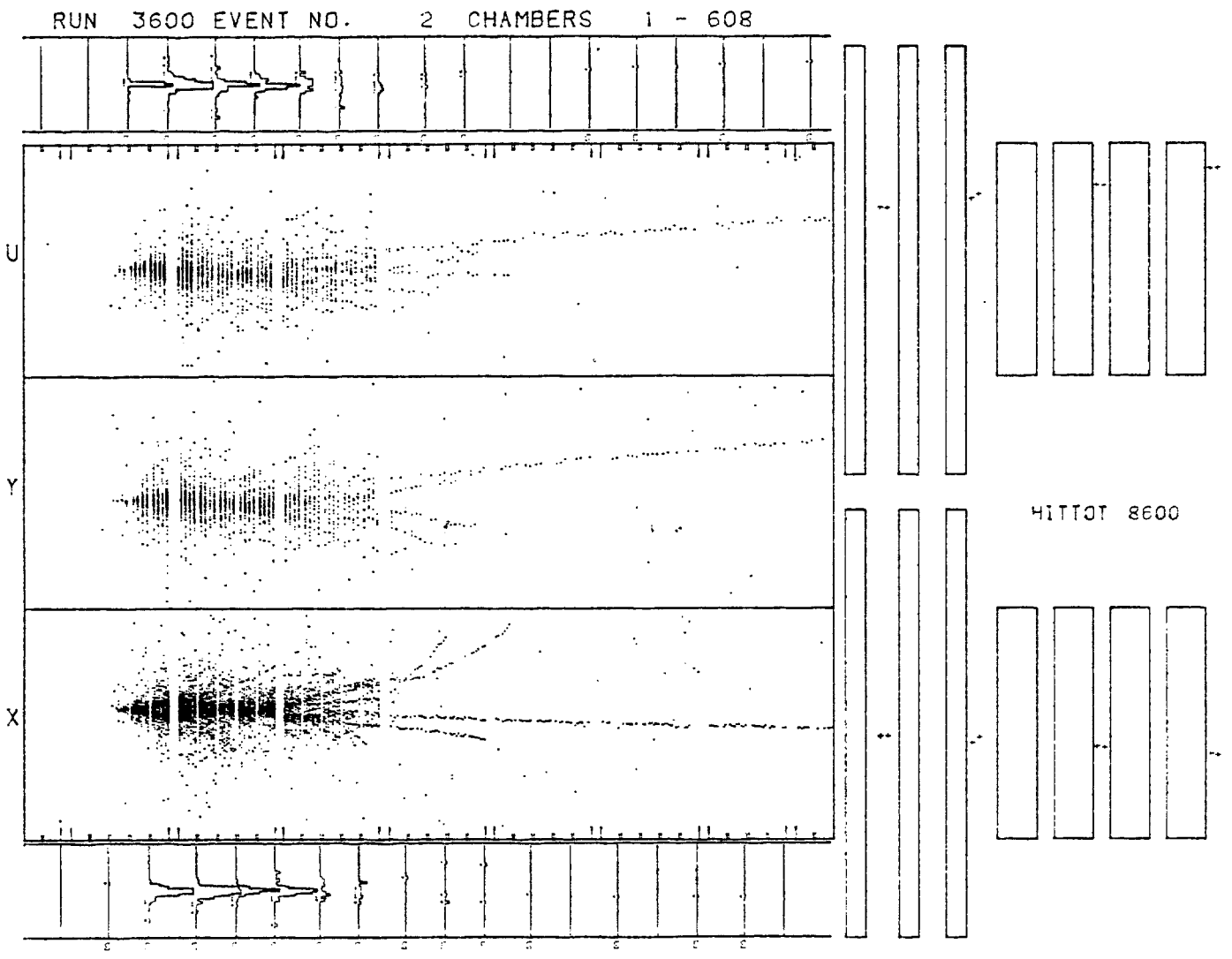

FIGURE A8a

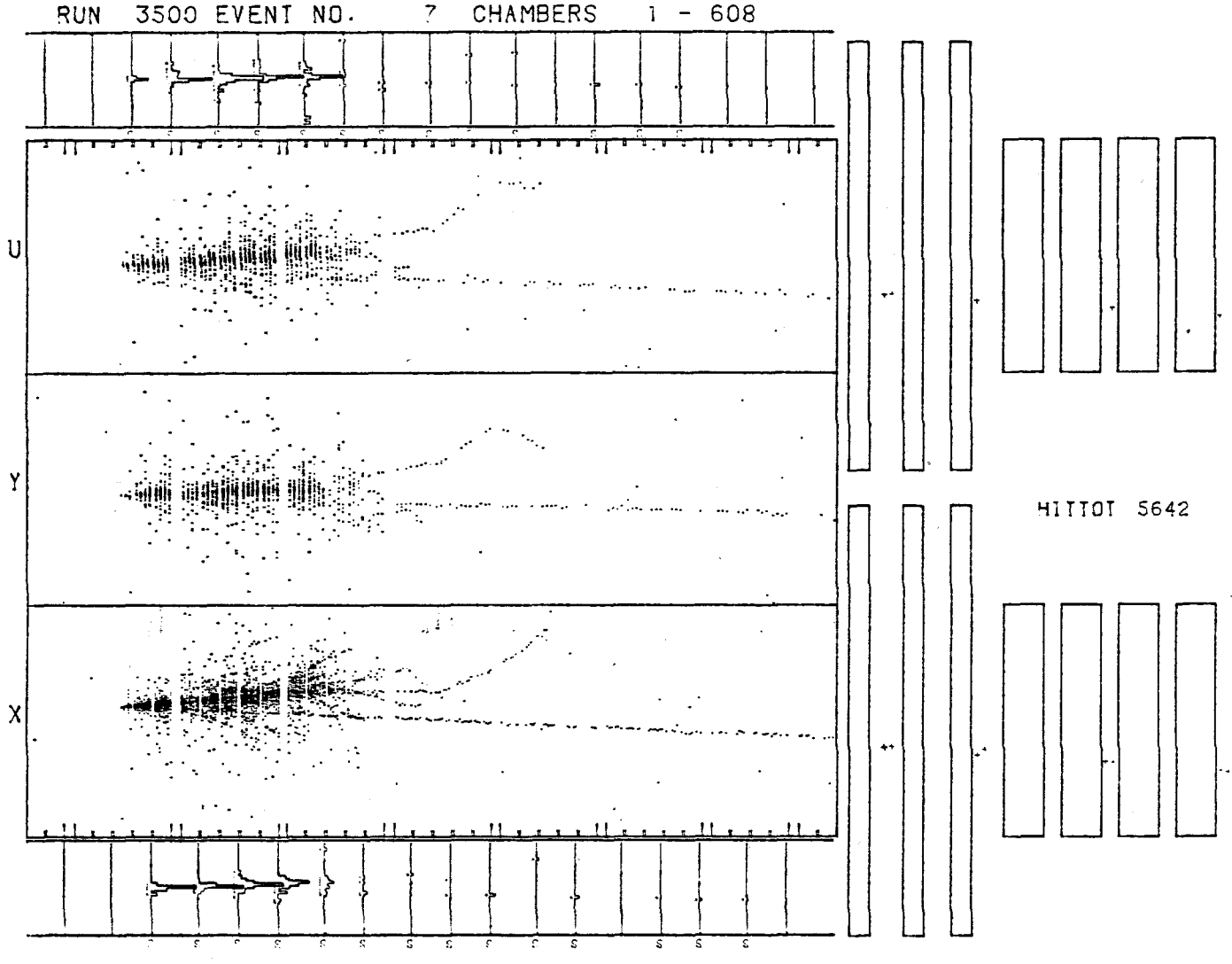

FIGURE A8b

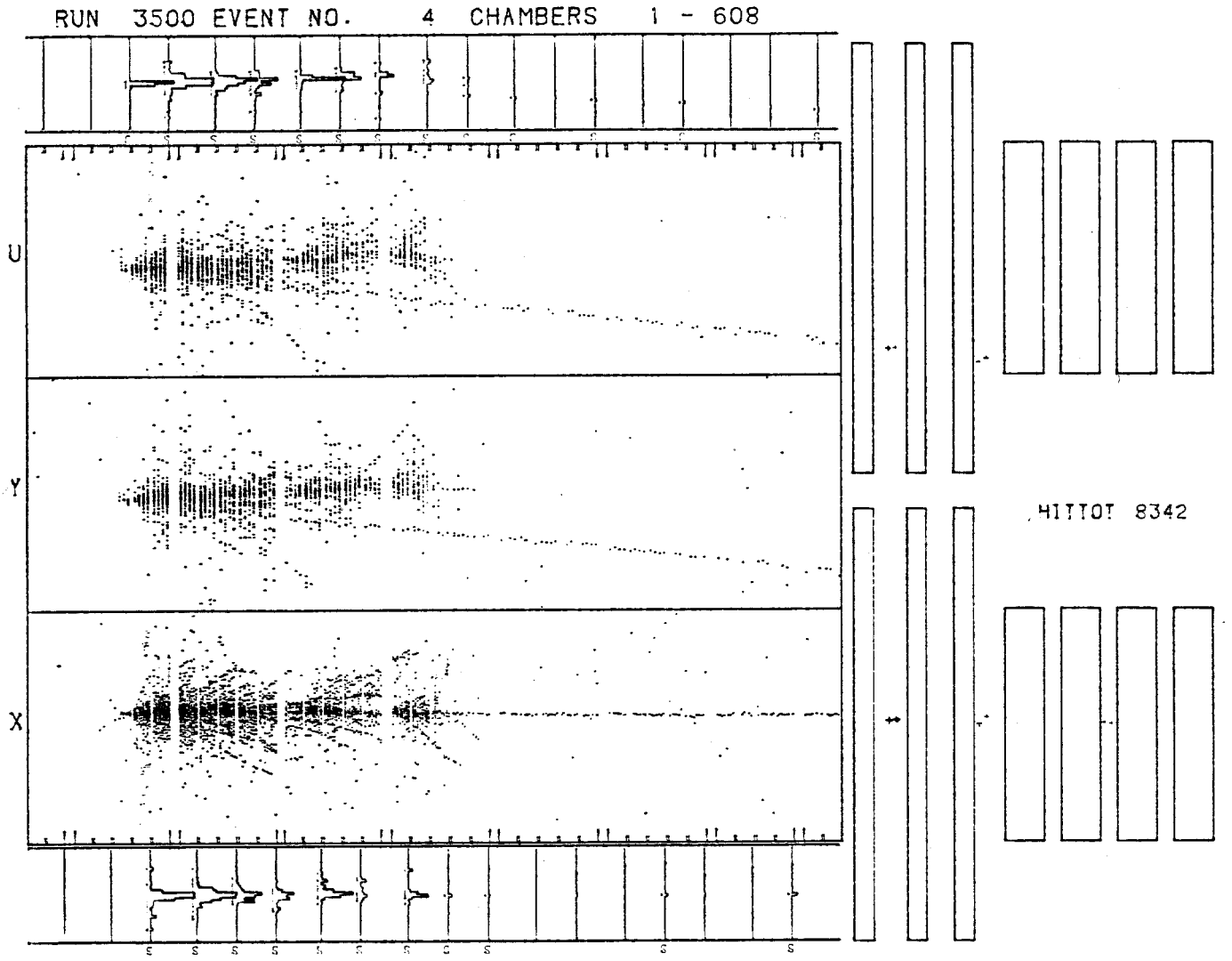

FIGURE A8c

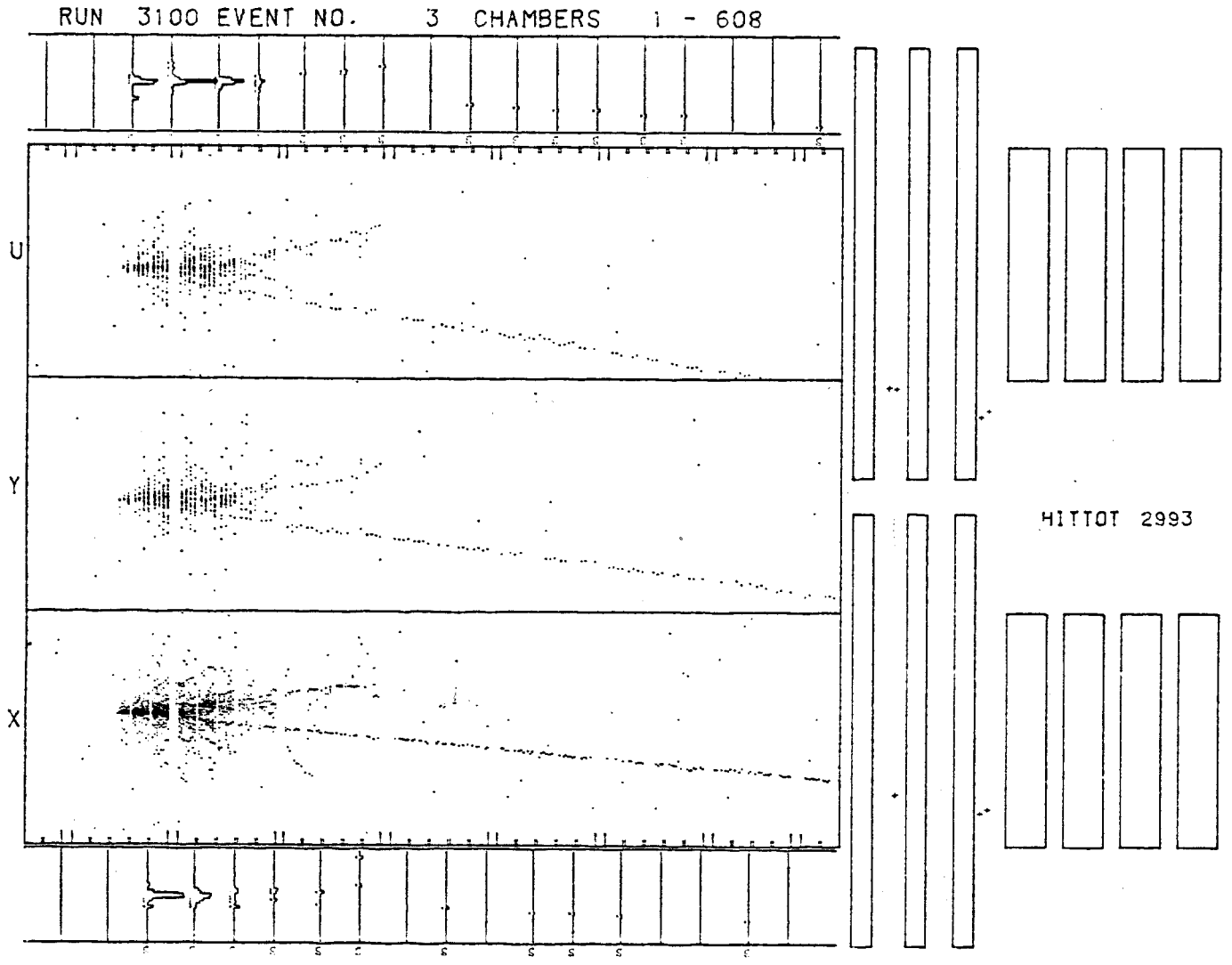

FIGURE A8d

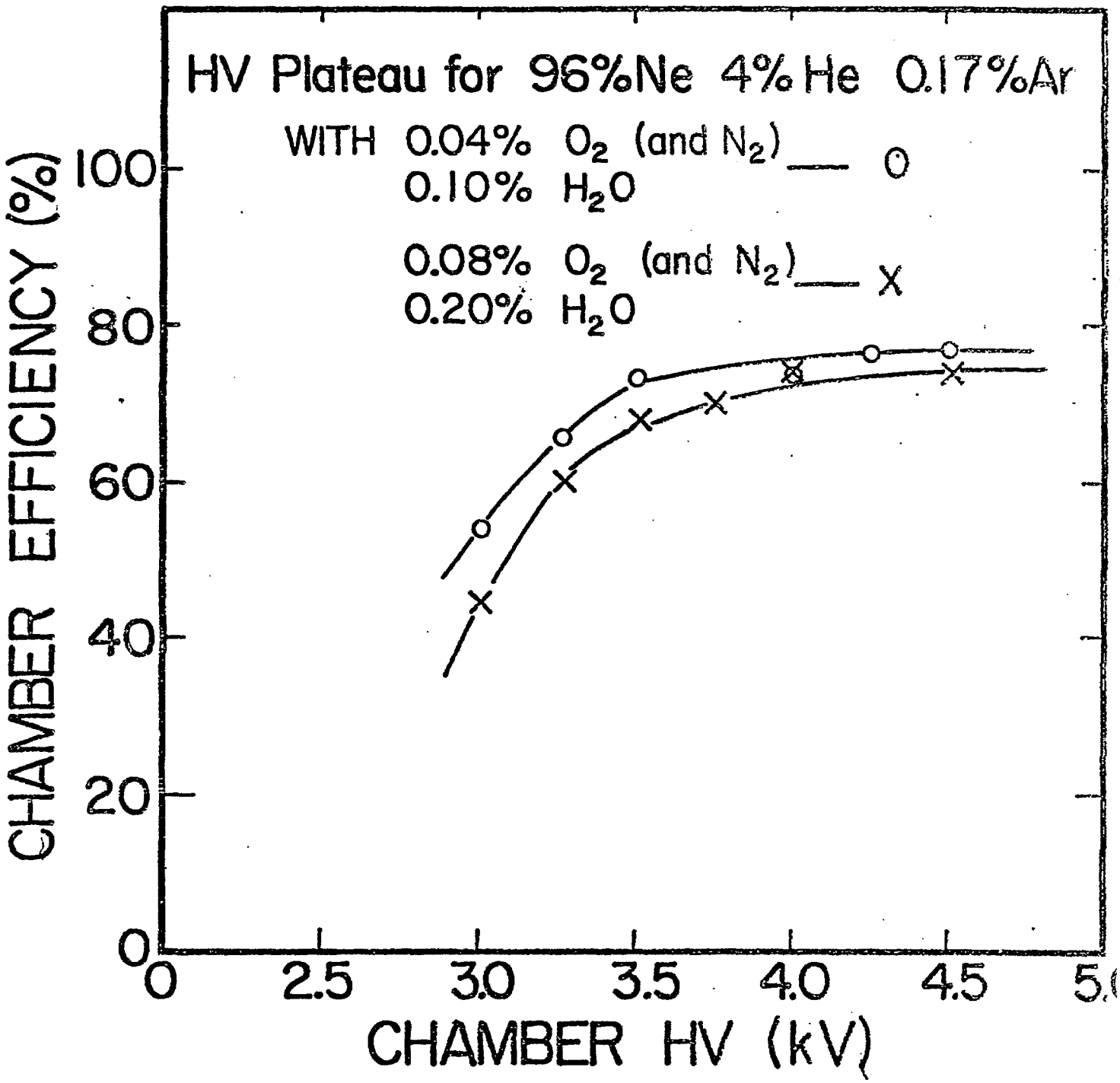
HV Plateau for 96%Ne 4%He 0.17%Ar
WITH 0.04% O_2 (and N_2) ___ O
0.10% H_2O
0.08% O_2 (and N_2) ___ X
0.20% H_2O
CHAMBER EFFICIENCY (%)
100
80
60
40
20
0
0
2.5
3.0
3.5
4.0
4.5
CHAMBER HV (kV)

FIGURE B1

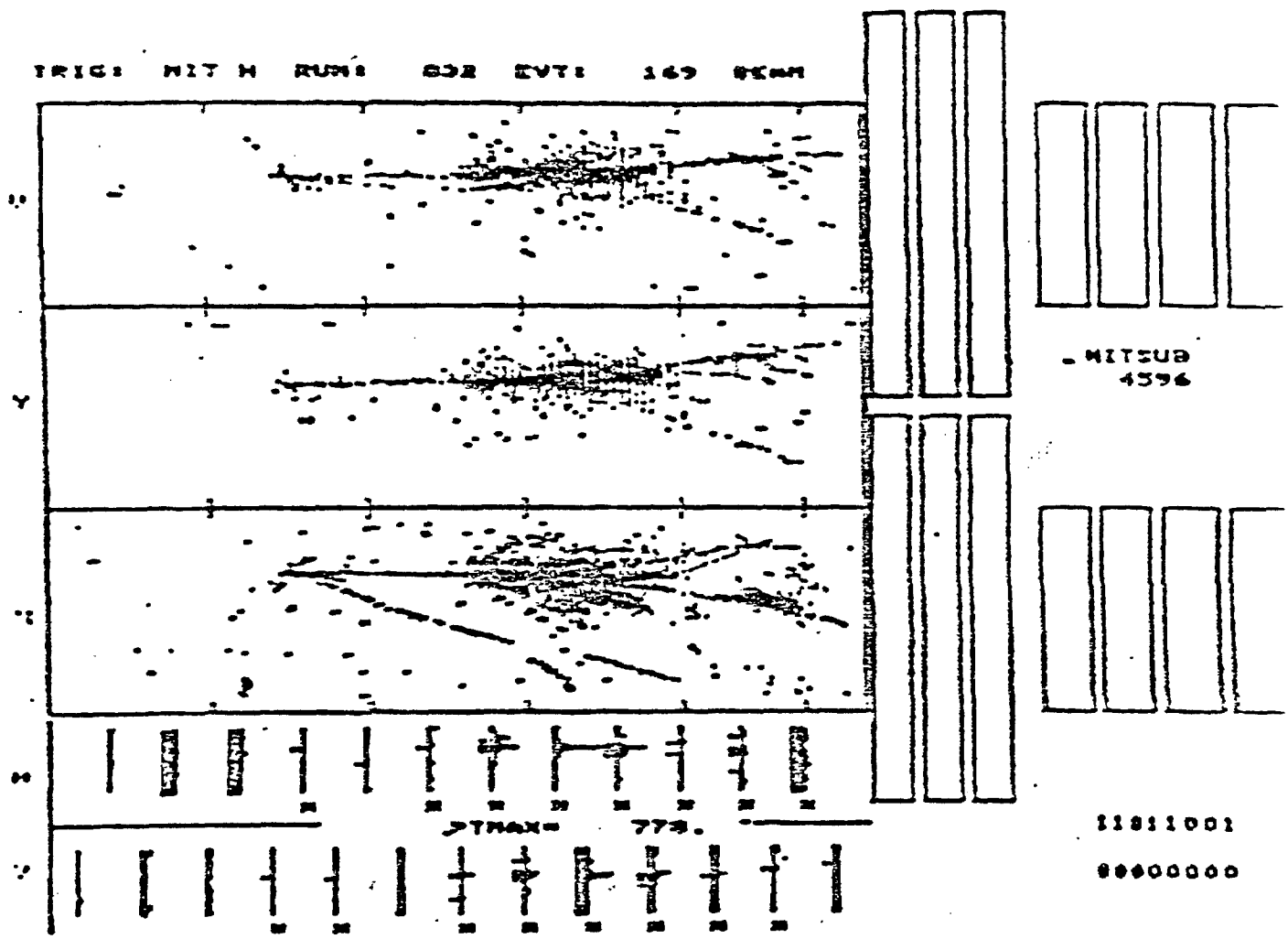
TRIG: MIT H RUN: 632 EVT: 169
MITSUB
4596
TMAX=
11011001
00000000

FIGURE A8g

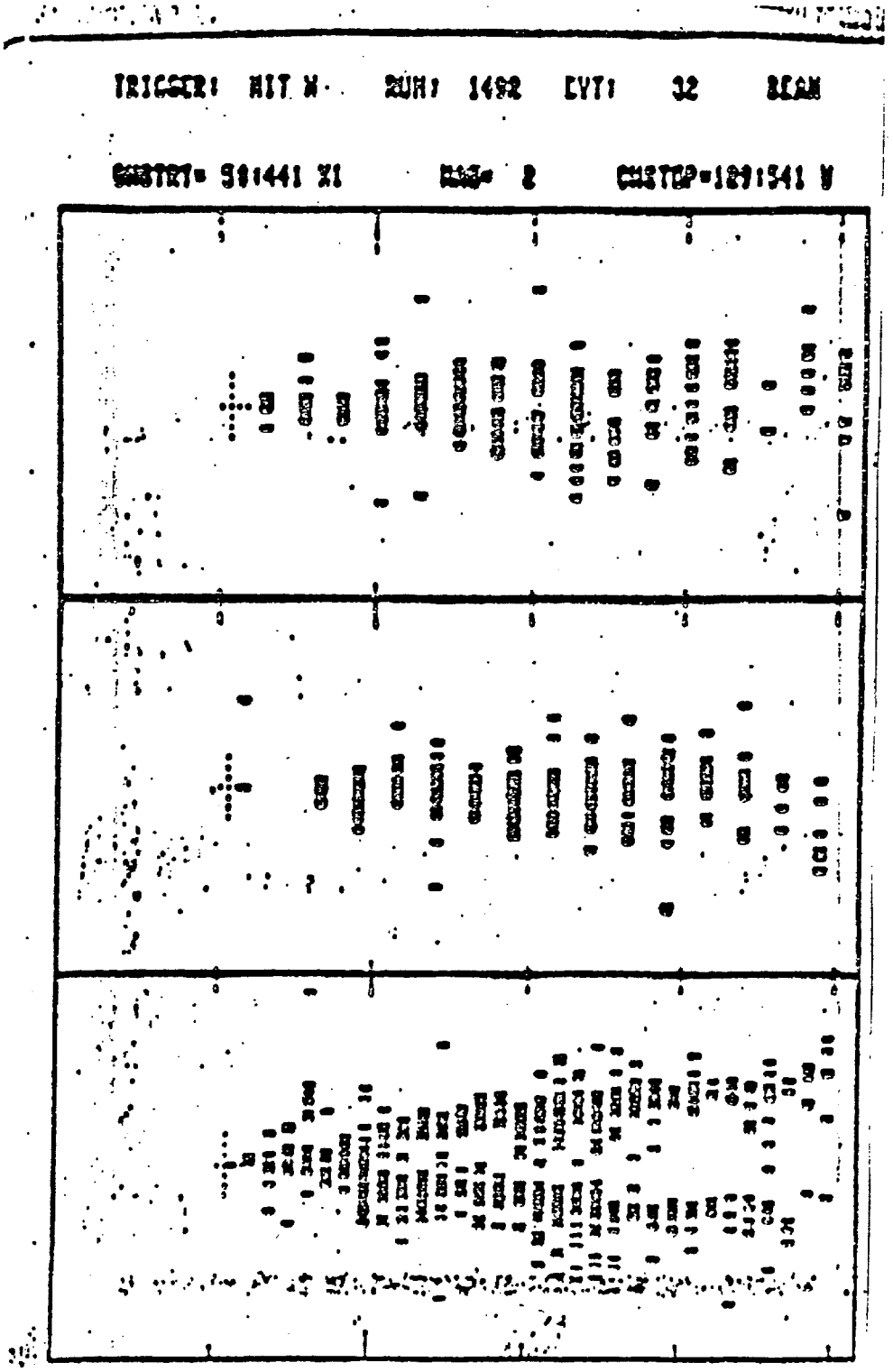

FIGURE A8h

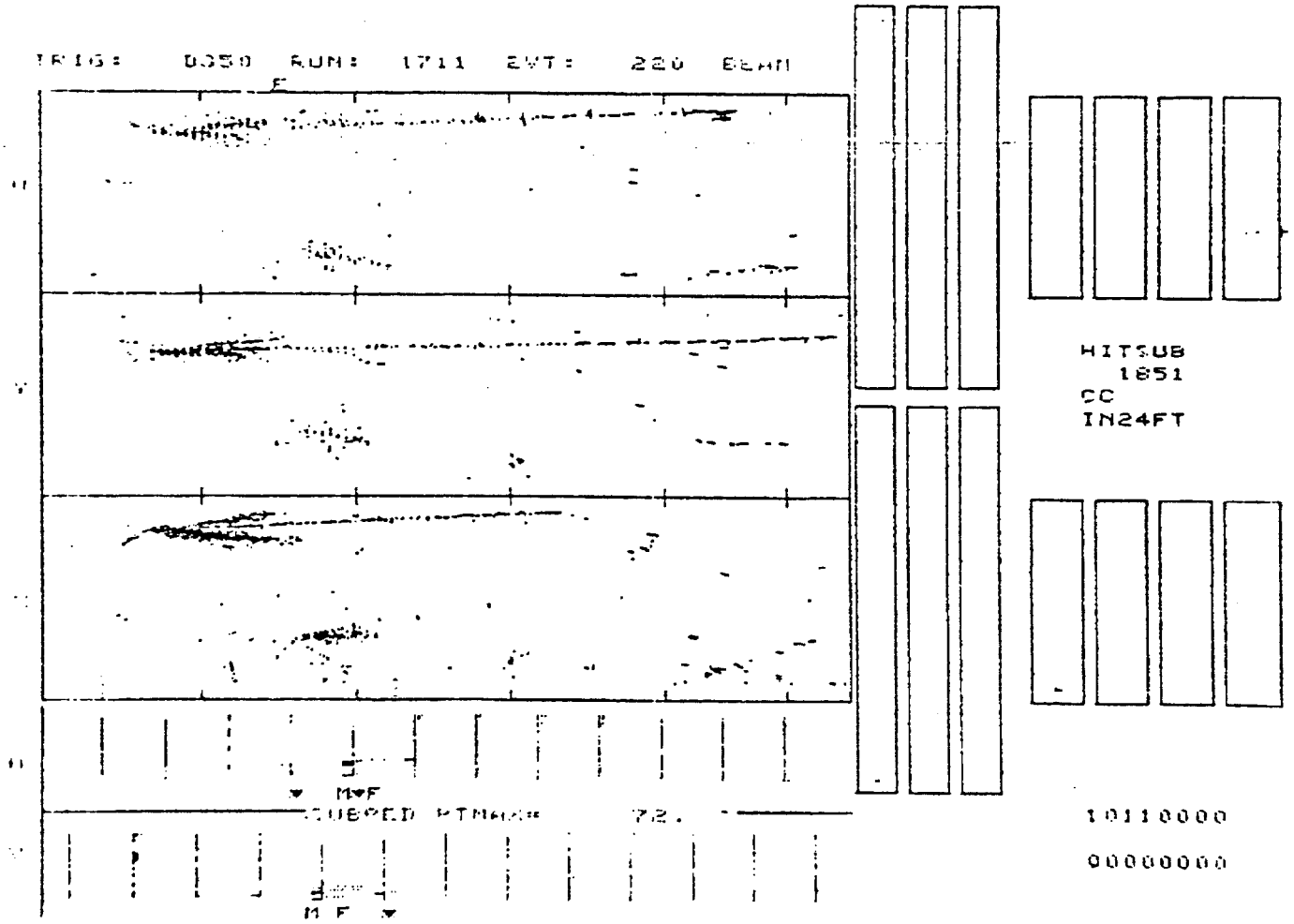
TRIG: 0350 RUN: 1711 EVT: 220 BEAM
HITSUB
1851
CC
IN24FT
10110000
00000000

FIGURE A8i

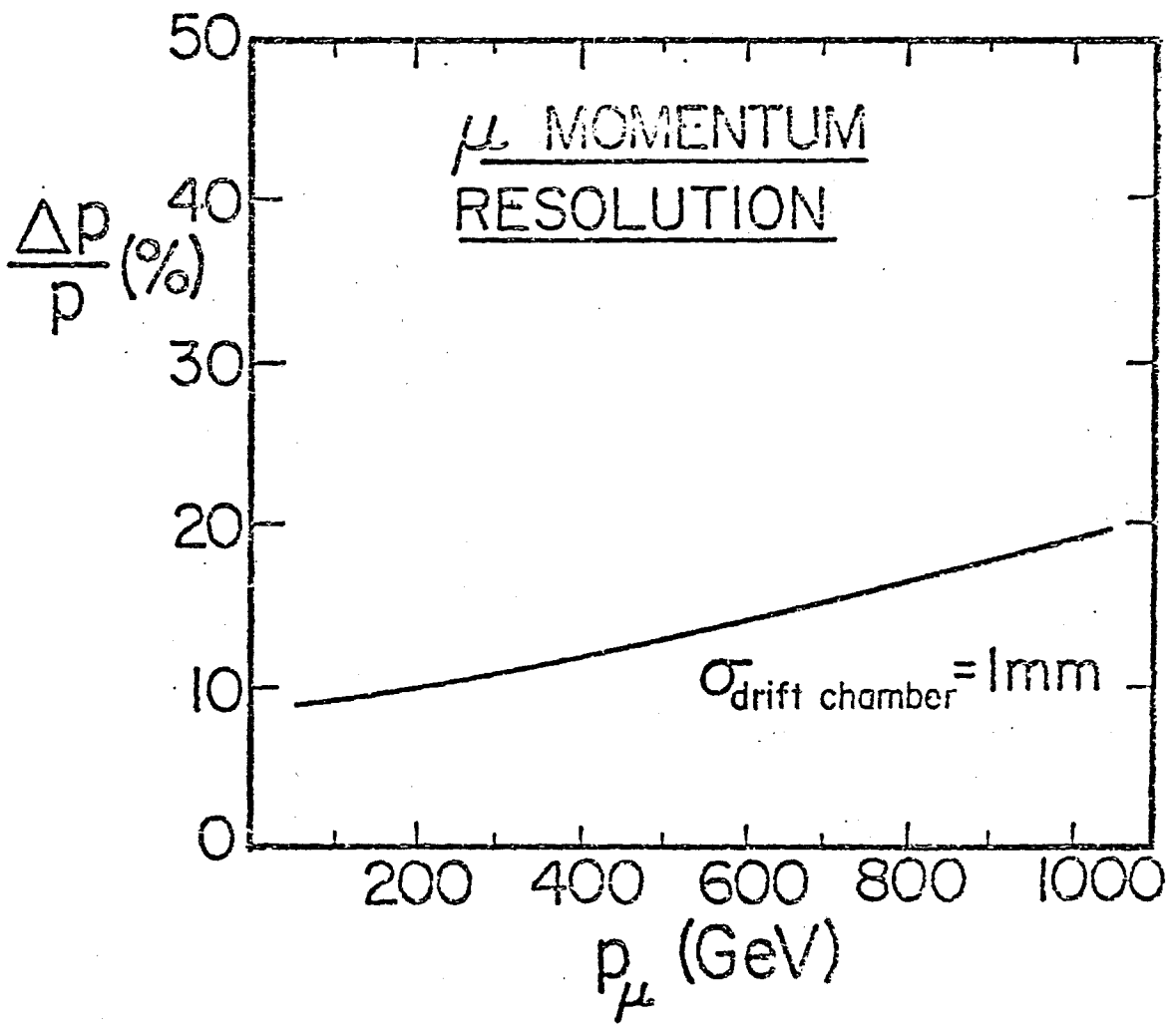
μ MOMENTUM
RESOLUTION
ΔP/P (%)
50
40
30
20
10
0
σdrift chamber = 1mm
200
400
600
800
1000
pμ (GeV)

FIGURE A9

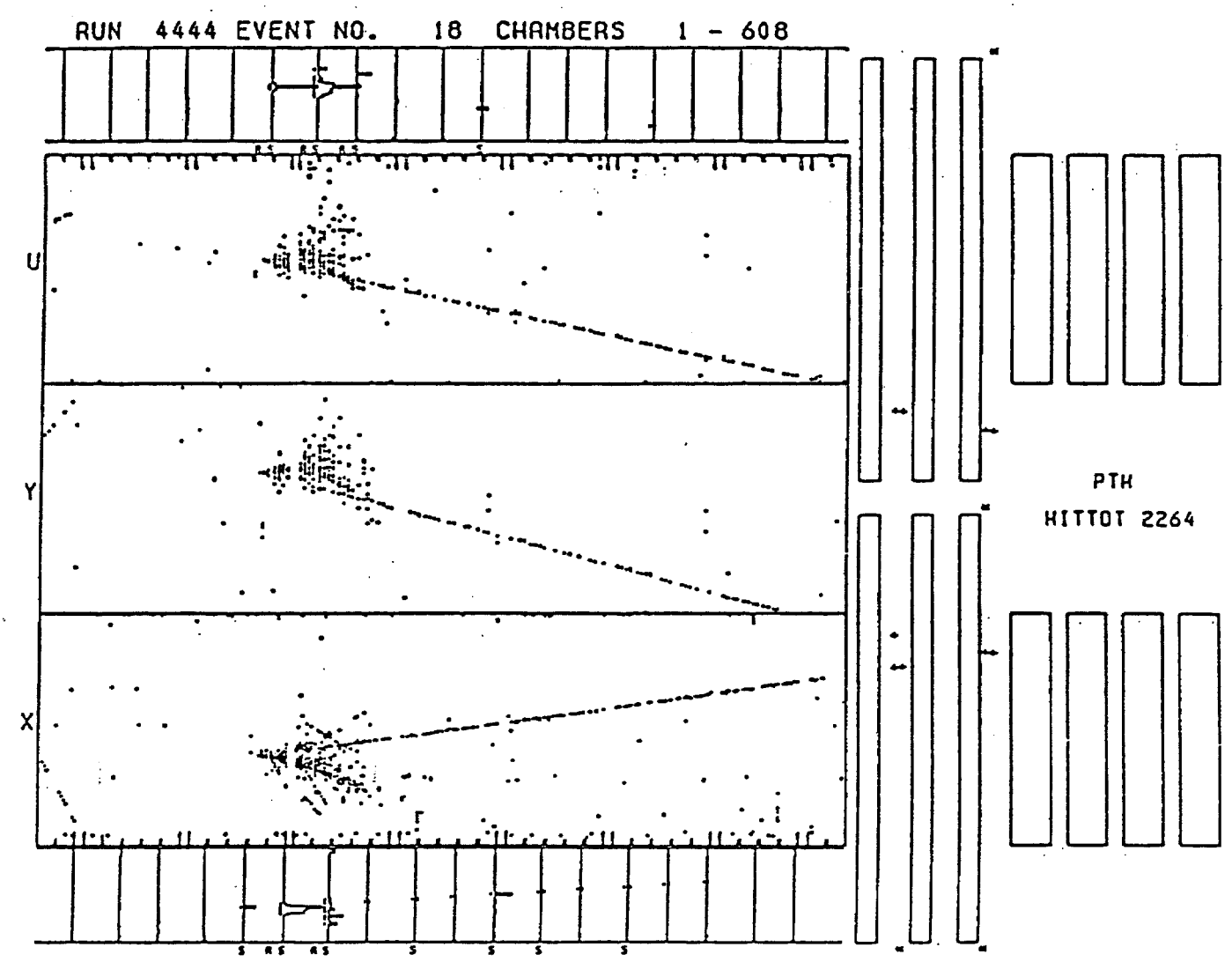

FIGURE A8e

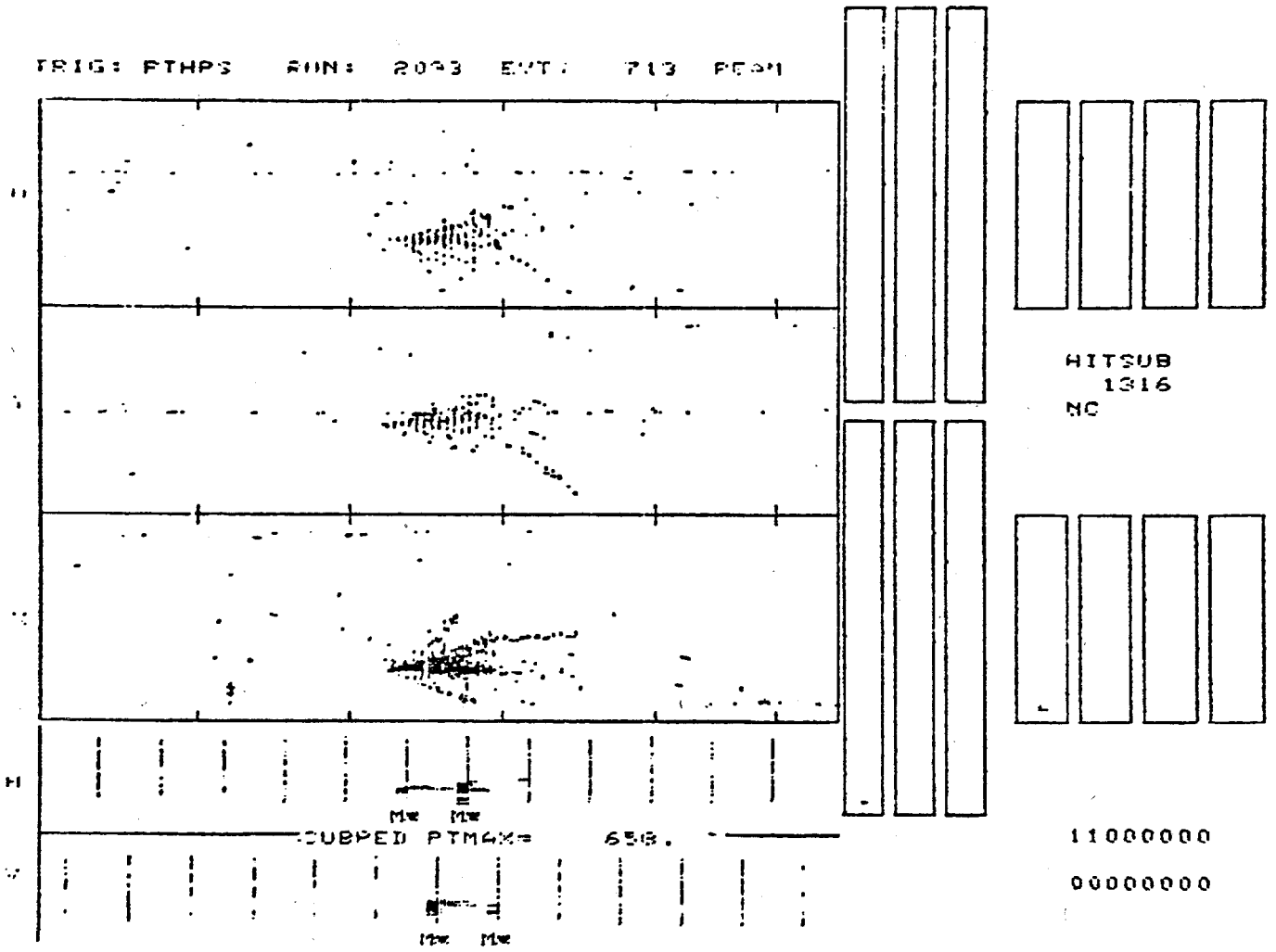
TRIG: PTHPS RUN: 2093 EVT: 713 PEAM
HITSUB
1316
NC
11000000
00000000

FIGURE A8f